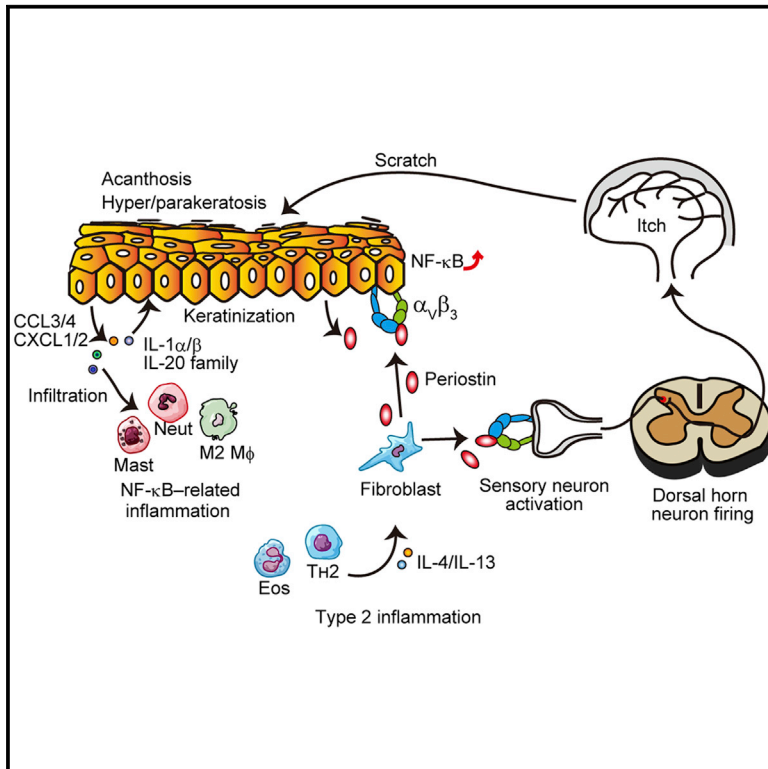


Periostin activates distinct modules of inflammation and itching downstream of the type 2 inflammation pathway

Graphical abstract



Authors

Satoshi Nunomura, Daisuke Uta, Isao Kitajima, ..., Tsugunobu Andoh, Simon J. Conway, Kenji Izuhara

Correspondence

nunomura@cc.saga-u.ac.jp (S.N.), kizuhara@cc.saga-u.ac.jp (K.I.)

In brief

Periostin, a downstream molecule of type 2 inflammation, plays a critical role in the pathogenesis of allergic skin inflammation. Nunomura et al. show that periostin links NF-κB-mediated inflammation with type 2 inflammation and promotes itching in allergic skin inflammation in the FADS mouse, a mouse model of AD.

Highlights

- Periostin links NF-κB-related inflammation with type 2 inflammation
- Periostin drives the spontaneous firing of dorsal horn neurons related with itching
- Pharmacological blockade of periostin suppresses skin inflammation and itching



Article

Periostin activates distinct modules of inflammation and itching downstream of the type 2 inflammation pathway

Satoshi Nunomura,^{1,6,*} Daisuke Uta,² Isao Kitajima,³ Yasuhiro Nanri,¹ Kosuke Matsuda,² Naoko Ejiri,³ Midori Kitajima,³ Hitoshi Ikemitsu,¹ Misaki Koga,¹ Sayaka Yamamoto,¹ Yuko Honda,¹ Hironobu Takedomi,¹ Tsugunobu Andoh,⁴ Simon J. Conway,⁵ and Kenji Izuhara^{1,*}

¹Division of Medical Biochemistry, Department of Biomolecular Sciences, Saga Medical School, 5-1-1, Nabeshima, Saga 849-8501, Japan

²Department of Applied Pharmacology, Faculty of Pharmaceutical Sciences, University of Toyama, Toyama 930-0194, Japan

³Department of Clinical Laboratory and Molecular Pathology, Graduate School of Medical and Pharmaceutical Science, University of Toyama, Toyama 930-0194, Japan

⁴Department of Pharmacology and Pathophysiology, College of Pharmacy, Kinjo Gakuin University, Nagoya 463-8521, Japan

⁵Herman B. Wells Center for Pediatric Research, Indiana University School of Medicine, Indianapolis, IN, USA

⁶Lead contact

*Correspondence: nunomura@cc.saga-u.ac.jp (S.N.), kizuhara@cc.saga-u.ac.jp (K.I.)

<https://doi.org/10.1016/j.celrep.2022.111933>

SUMMARY

Atopic dermatitis (AD) is a chronic relapsing skin disease accompanied by recurrent itching. Although type 2 inflammation is dominant in allergic skin inflammation, it is not fully understood how non-type 2 inflammation co-exists with type 2 inflammation or how type 2 inflammation causes itching. We have recently established the FADS mouse, a mouse model of AD. In FADS mice, either genetic disruption or pharmacological inhibition of periostin, a downstream molecule of type 2 inflammation, inhibits NF- κ B activation in keratinocytes, leading to downregulating eczema, epidermal hyperplasia, and infiltration of neutrophils, without regulating the enhanced type 2 inflammation. Moreover, inhibition of periostin blocks spontaneous firing of superficial dorsal horn neurons followed by a decrease in scratching behaviors due to itching. Taken together, periostin links NF- κ B-mediated inflammation with type 2 inflammation and promotes itching in allergic skin inflammation, suggesting that periostin is a promising therapeutic target for AD.

INTRODUCTION

Atopic dermatitis (AD) is a chronic relapsing skin disease with persistent pruritus.¹ It is widely accepted that type 2 inflammation is dominant in the pathogenesis of AD. Based on this notion, several therapeutic agents targeting type 2 cytokines such as dupilumab have been or are now being developed.^{2,3} However, it is also known that high expression of other types of inflammatory responses—type 1/type 17/type 22 inflammation as well as nuclear factor (NF)- κ B-mediated inflammation—are accompanied by type 2 inflammation in skin lesions of patients with AD.^{4–7} Importantly, patients showing the expression profile combining type 2 cytokines and non-type 2 cytokines have clinically more severe AD than patients with type 2 cytokines alone.^{7–10} Moreover, it has been reported that in patients with AD, high co-expression of type 2 and non-type 2 cytokines is correlated with resistance to topical steroid therapy.¹¹ These findings suggest that the involvement of non-type 2 inflammation in the pathogenesis of AD affects its clinical severity. However, it remains unclear how type 2 inflammation and non-type 2 inflammation co-exist in the pathogenesis of AD and precisely what role is played by non-type 2 inflammation.

Chronic recurrent itching is a hallmark of AD, disturbing quality of life, including sleep and social activities, for patients with AD.¹² Moreover, itch-mediated scratching behaviors worsen the skin barrier disruption, followed by exacerbating type 2 inflammation in the pathogenesis of AD.¹³ Therefore, to better treat patients with AD, it is important to clarify the molecular mechanism of itching and to establish a way to control it. The molecular mechanism of itch transduction through peripheral responses to pruritogens has been well characterized in recent decades.^{14,15} Pruritogens produced in the skin lesions of patients with AD activate peripheral sensory neurons such as dorsal root ganglia (DRG) neurons, promoting the opening of calcium-permeable ion channels, such as transit receptor potential vanilloid 1 (TRPV1) and ankyrin 1 (TRPA1), leading to itching.¹⁶ Itch signals are then processed in the superficial dorsal horn neurons of the spinal cord and are conveyed to the thalamus and the parabrachial nucleus. They are then projected into various areas in the central nervous system. It has recently been revealed that mouse non-peptidergic 2 (NP2) and NP3 type neurons express various type 2 cytokine receptors for interleukin 4 (IL-4), IL-13, IL-31, and IL-33, as well as thymic stromal lymphopoietin (TSLP).¹⁵ These cytokines produced in the skin lesions of patients with AD then



activate TRPV1 and/or TRPA1 on these nerve cells via their cytosolic receptors.^{17–20} Therefore, we need greater clarification of exactly how type 2 inflammation is linked to the activation of peripheral nerve cells for itching.

Periostin is a matricellular protein belonging to the fasciclin family, transducing the signals in the cells by interacting with cell surface integrins such as $\alpha_V\beta_3$ or $\alpha_V\beta_5$.^{21,22} We have previously demonstrated that periostin is a downstream molecule of IL-4 and IL-13 signals and is highly expressed in the dermis of skin lesions of patients with AD.^{23,24} Moreover, we have shown that serum periostin is high in patients with AD correlated with their clinical severities, suggesting that serum periostin would be a useful biomarker for their treatment.²⁵ Genetic deficiency of periostin diminished mite-induced allergic skin inflammation in mice.²³ Moreover, we have confirmed by the three-dimensional organotypic coculture system using keratinocytes and fibroblasts that periostin derived from fibroblasts binds to $\alpha_V\beta_3/\alpha_V\beta_5$ on keratinocytes, activating NF- κ B followed by inducing pro-inflammatory mediators, including TSLP.^{23,26} These findings suggest that periostin is critical in the pathogenesis of AD, accelerating type 2 inflammation. However, it remains elusive whether periostin is important for the onset of non-type 2 inflammation. Furthermore, it has recently been demonstrated that the injection of periostin triggered scratch behaviors in mice, dogs, and monkeys and that periostin directly activated DRG sensory neurons via $\alpha_V\beta_3$ integrin, highlighting a role for periostin in AD pathogenesis as a pruritogen.²⁷ The observation in prurigo nodularis, a type 2 inflammation-prone itchy skin, that the periostin expression levels are positively correlated with itching intensity supports this notion.²⁸ Therefore, the precise role of periostin in the pathogenesis of AD awaits clarification, looking at overall inflammation as well as itching, using an appropriate *in vivo* model.

We have recently established a mouse model of AD named facial atopic dermatitis with scratching (FADS) mouse by selectively deleting *Ikk2*, a positive regulator for the NF- κ B signaling, under the control of nestin expression.^{29,30} FADS mice exhibit eczema lesions limited to the face, probably because of the expression of nestin in facial dermal fibroblasts derived from neural crest cells. Facial skin lesions of FADS mice show a high expression profile of type 2 inflammation-related genes (*Il4*, *Il5*, *Il9*, *Il13*, and *Tslp*) and the gene expression profile is very similar to that of patients with AD compared with other mouse models of AD. It is of note that the expression of periostin, a downstream molecule of type 2 inflammation, is upregulated in the dermis of the skin lesions and in blood.²⁹ These results demonstrate that the pathogenesis of FADS mouse is similar to that of patients with AD.²⁹ Moreover, expression of non-type 2 inflammation-related molecules in addition to type 2 inflammation type 17 family gene (*Il17a*), and the NF- κ B-related cytokines (IL-10/20 family genes: *Il10*, *Il19*, *Il20*, and *Il24*; IL-1 family genes: *Il1b*, *Il18*, *Il36a*, *Il36b*, and *Il36g*; and pro-inflammatory genes: *Il6*, and *Tnf*) is also upregulated in face skins of FADS mice. These results suggest that, although it remains unclear how genetic disruption of *Ikk2* in dermal fibroblasts causes AD-like phenotypes, the FADS mouse model is suitable for analyzing the correlation between type 2 and non-type 2 inflammation in the pathogenesis of AD. Moreover, FADS mice exhibit spontaneous, severe scratching behaviors because of itching, so it is a useful

in vivo model for clarifying the molecular mechanism of itching in AD pathogenesis and to develop or evaluate therapeutic agents for itching. The finding of high periostin expression in FADS mice raises the possibility that periostin is involved in the setting of inflammation and itching in these mice.

In this study, we investigated the functional role of periostin in the pathogenesis of AD using our FADS mouse, taking both genetic and pharmacological approaches and finding that periostin plays a critical role in activating NF- κ B in keratinocytes. In other words, periostin links NF- κ B-mediated inflammation with type 2 inflammation in the FADS mouse. Moreover, we confirmed that in FADS mice, periostin causes spontaneous firing of itch-related neurons, followed by enhancing scratching behaviors due to itching. These results provide us with a greater understanding of the mechanism behind the pathogenesis of AD, as well as a promising strategy for treating patients with AD targeting periostin.

RESULTS

Infiltration of both eosinophils and neutrophils together with high expression of periostin in the facial skin of FADS mice

FADS/*Postn*^{+/+} mice showed eczema restricted to the face (Figure 1A), histological findings similar to patients with AD—acanthosis with spongiosis, hyper- and parakeratosis, and accumulation of eosinophils and mast cells in the dermis (Figure 1B)—and high expression of periostin dominant in the dermis and slightly in the epidermis (Figures 1C and 1D), as demonstrated earlier.²⁹ We previously demonstrated that in FADS mice, expression of non-type 2 cytokines—type 17 inflammation-related gene (*Il17a*), and the NF- κ B-related cytokines including the IL-10/20 family of genes (*Il10*, *Il19*, *Il20*, and *Il24*), IL-1 family of genes (*Il1b*, *Il18*, *Il36a*, *Il36b*, and *Il36g*), and pro-inflammatory genes (*Il6* and *Tnf*)—is upregulated in addition to type 2 inflammation-related genes (*Il4*, *Il5*, and *Il13*).²⁹ We investigated whether skin lesions in FADS mice histologically reflect such combined immunologic abnormalities. We found that neutrophils, the effector cells of non-type 2 inflammation, infiltrated dominantly into the dermis in FADS/*Postn*^{+/+} mice, and to a lesser extent in the epidermis (Figure 1E). Neutrophils as well as eosinophils infiltrated into the dermis area with the expression of periostin (Figure 1F). These results demonstrate that, in the facial skin of FADS mice, both eosinophils and neutrophils are infiltrated together, reflecting high expression of type 2 and non-type 2 cytokines with high expression of periostin.

Identification of periostin-producing cells in the skin lesions of FADS mice

We have previously demonstrated that fibroblasts are the main periostin-producing cells in AD skin lesions,²³ and it has been shown that periostin is expressed in COL6A5⁺COL18A1⁺ fibroblasts.³¹ In addition to fibroblasts, keratinocytes, vascular endothelial cells, and mast cells have been reported to have the potential to express periostin.^{32–34} To identify periostin-producing cells in FADS mice, we generated FADS/*Postn*^{lacZ/+} mice, in which the *Postn* gene is replaced with the lacZ reporter gene in a heterogeneous manner. The β -galactosidase (β -gal)-positive cells were increased in PDGFR α ⁺ dermal cells and to a lesser

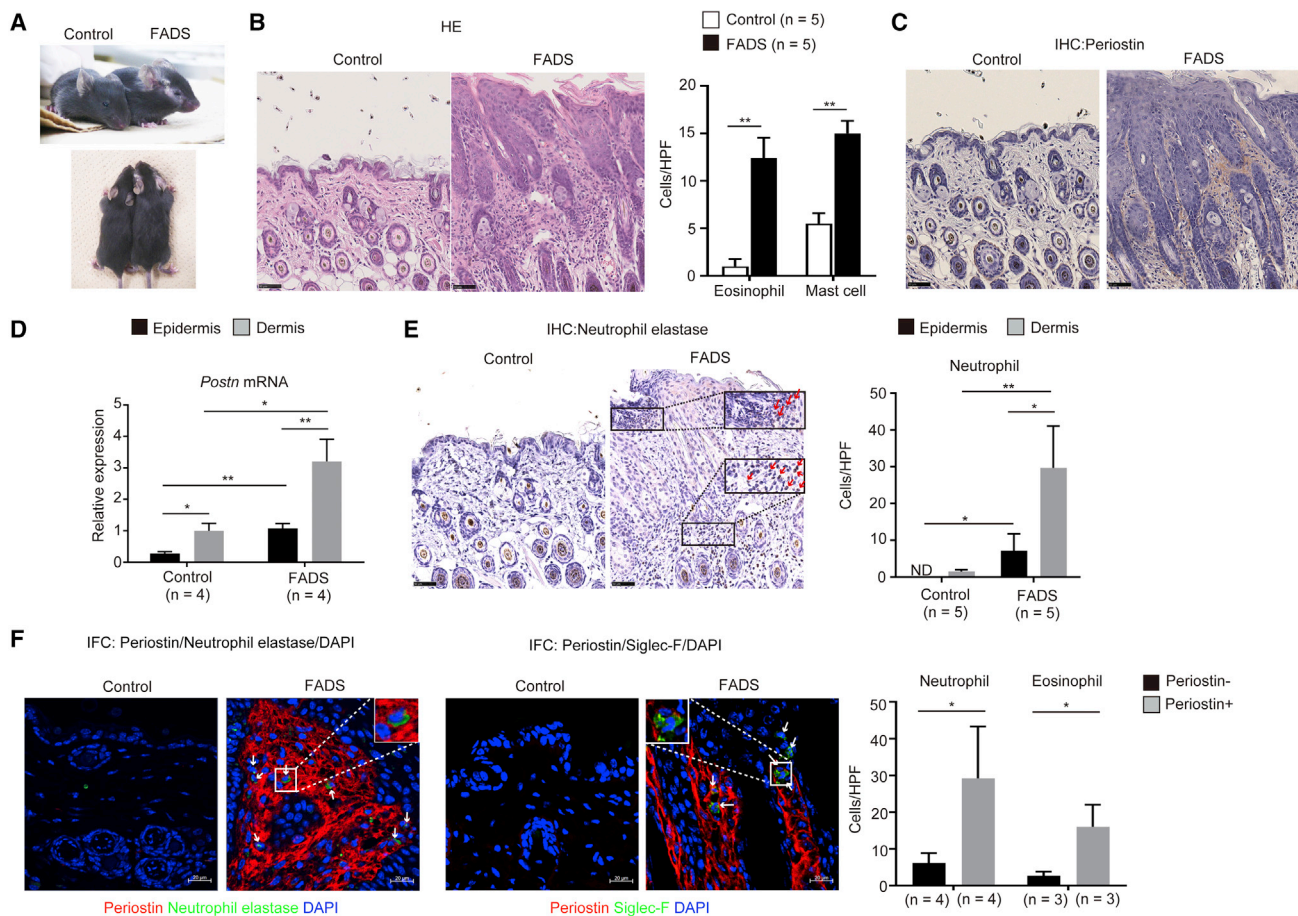


Figure 1. Infiltration of both eosinophils and neutrophils together with high expression of periostin in the facial skin of FADS mice

(A) Macroscopic facial skin lesions of 4-week-old FADS/*Postn*^{+/+} and control/*Postn*^{+/+} mice. (B, C, and E) Hematoxylin and eosin (HE) (B), periostin (C), and neutrophil elastase (E) staining of facial skin of FADS/*Postn*^{+/+} mice (n = 5) and control/*Postn*^{+/+} mice (n = 5). Red arrows indicate neutrophils (E). The numbers per high-power field (HPF; ×40) of eosinophils and mast cells in the dermis (B) and neutrophils (E) in the epidermis and in the dermis are depicted. (D) Quantitative real-time PCR analysis for periostin of 4-week-old FADS/*Postn*^{+/+} mice (n = 4) and control/*Postn*^{+/+} mice (n = 4). The relative mRNA expression levels of periostin were normalized to *Gapdh*, and the mean expression levels for the dermis of control/*Postn*^{+/+} mice are displayed as 1. (F) Double immunostaining for neutrophil elastase and periostin (left) or siglec-F and periostin (right) of facial skin of FADS/*Postn*^{+/+} mice (n = 3–4) and control/*Postn*^{+/+} mice (n = 3–4). The numbers per HPF (×40) of neutrophils and eosinophils in the dermis area with or without periostin expression are depicted. White arrows indicate neutrophils (left) or eosinophils (right). Scale bars: 50 μm (B, C, and E) and 20 μm (F). The data shown are the mean ± standard deviation (D) or standard error of the mean (B, E, and F) of samples obtained from three independent experiments. Statistical analysis was performed using a two-sided Student t-test (D) or a one-sided Mann-Whitney U-test (B, E, F); *p < 0.05, **p < 0.01. IHC, immunohistochemistry.

extent in EpCAM⁺ epidermal cells of FADS mice compared with those of control mice, but not in either CD31⁺ endothelial cells or CD45.2⁺ leukocytes (Figure 2A). These results suggest that fibroblasts and keratinocytes are the periostin-producing cells in FADS mice.

We have previously demonstrated that facial dermal fibroblasts are heterogeneous and that *Ikk2* is deleted in the neural crest cell-derived fibroblasts in which nestin is exclusively expressed in FADS mice.²⁹ We next examined whether periostin-producing dermal fibroblasts overlap with nestin-expressing or *Ikk2*-deleted dermal fibroblasts in FADS mice using FADS/*Postn*^{lacZ/+}/*Rosa26*^{RFP/+} mice. We found that, although the cells with high β-gal activity (periostin-expressing cells) were increased in FADS mice compared with control mice, these cells were distrib-

uted in both the RFP⁺ population (*Ikk2*-non-expressing cells) and the RFP⁻ population (*Ikk2*-expressing cells) in PDGFRα⁺ dermal fibroblasts (Figure 2B). Moreover, when we incubated two kinds of primary cultured dermal fibroblasts derived from FADS/*Postn*^{lacZ/+}/*Rosa26*^{RFP/+} mice—RFP⁺ cells and RFP⁻ cells—with IL-13, both types of cells showed enhanced β-gal expression (Figure 2C). These results demonstrate that distributions of periostin and *Ikk2* are not the same in facial dermal fibroblasts and that periostin is expressed in both *Ikk2*⁺ and *Ikk2*⁻ dermal fibroblasts.

Improvement of the progression of skin inflammation by genetic disruption of periostin in FADS mice

To elucidate the functional roles of periostin in the onset or progression of skin inflammation in FADS mice, we applied a genetic

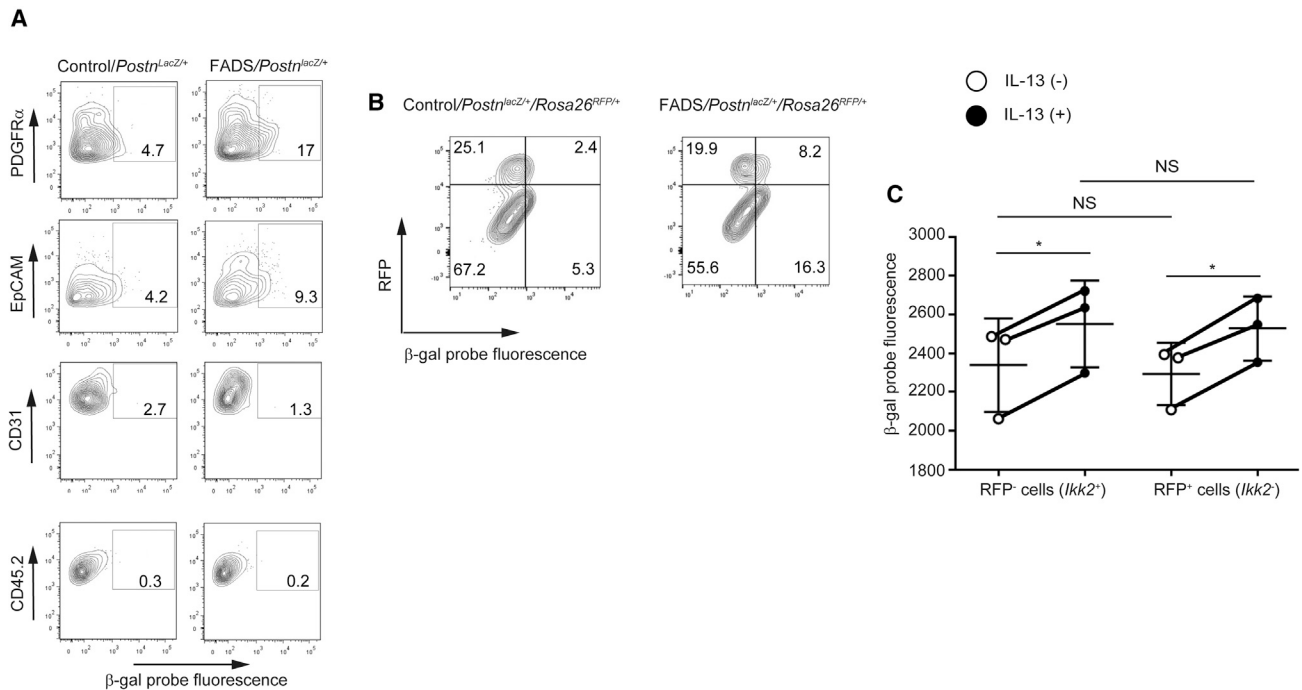


Figure 2. Identification of periostin-producing cells in the skin lesions of FADS mice

(A) β -Gal-positive cells in PDGFR α ⁺ and EpCAM⁺ facial dermal cells of 4-week-old FADS/*Postn^{lacZ/+}* mice and control/*Postn^{lacZ/+}* mice. PDGFR α ⁻, EpCAM⁻, CD31⁻, and CD45.2⁻-gated cells are depicted.

(B) β -Gal-positive cells in both RFP⁺PDGFR α ⁺ and RFP⁻PDGFR α ⁺ cells derived from 4-week-old FADS/*Postn^{lacZ/+}*/*Rosa26^{RFP/+}* mice and control/*Postn^{lacZ/+}*/*Rosa26^{RFP/+}* mice.

(C) β -Gal expression by treatment with or without 50 ng/mL IL-13 for 24 h in both RFP⁻ (*Ik2*⁻) and RFP⁺ (*Ik2*⁺) primary cultured dermal fibroblasts. The data shown are the mean \pm standard error of the mean of three fibroblast samples prepared separately from three mice. Similar results were obtained from three separate experiments. Statistical analysis was performed using a two-sided, paired Student t-test; **p* < 0.05, ***p* < 0.01. NS, not significant.

approach to disrupt periostin by generating FADS/*Postn^{lacZ/lacZ}* mice. We confirmed disruption of the *Postn* gene and the periostin expression in the dermis of the facial skin in FADS/*Postn^{lacZ/lacZ}* mice (Figure S1). Periostin deficiency did not prevent the onset of facial eczema; it appeared around postnatal day 10; it also did in the control mice (Figures 3A and S2). However, eczema did not develop thereafter, and the eczema was significantly improved compared with FADS/*Postn^{+/+}* mice at both P17 and P28 in FADS/*Postn^{lacZ/lacZ}* mice (Figure 3A). Histological analysis at postnatal day 28 showed reduced epidermal hyperplasia and dermis swelling (Figures 3B and 3C), decrease of neutrophils, mast cells, and F4/80⁺CD163⁺ M2 macrophages in FADS/*Postn^{lacZ/lacZ}* mice (Figures 3D–3G), whereas the numbers of eosinophils and basophils were not altered compared with FADS/*Postn^{+/+}* mice (Figures 3D–3G). These data suggest that, in FADS mice, periostin is critical for the progression, but not the onset, of skin inflammation, including eczema, epidermal and dermal thickness, and the infiltration of neutrophils, mast cells, and M2 macrophages, but not of eosinophils and basophils.

Requirement of periostin for expression of the NF- κ B-related cytokines and chemokines related to neutrophil migration in FADS mice

To clarify how genetic disruption of periostin improves skin inflammation in FADS mice, we compared the expression

profiles of inflammatory cytokine and chemokine genes. FADS/*Postn^{lacZ/lacZ}* mice showed expression comparable with or higher than FADS/*Postn^{+/+}* mice in type 2 cytokines *Il4*, *Il5*, and *Il13*; a type 17 cytokine, *Il17a*; and the type 2 inflammation-related chemokines *Ccl11*, *Ccl17*, and *Ccl24* (Figure 3H). In contrast, the expression of NF- κ B-related cytokines—*Il1b*, *Il24*, and *Il33*—and chemokines related to neutrophil migration—*Ccl3*, *Ccl4*, and *Cxcl2*—was significantly downregulated in FADS/*Postn^{lacZ/lacZ}* mice. Expression of other NF- κ B-related cytokines and chemokines related to neutrophil migration—*Il1a*, *Il6*, *Il19*, *Il20*, *Tslp*, and *Cxcl1*—tended to be downregulated in FADS/*Postn^{lacZ/lacZ}* mice, although it was not statistically significant. These results demonstrate that periostin is required for expression of NF- κ B-related cytokines and chemokines related to neutrophil migration, but not the expression of type 2 cytokines and chemokines related to the infiltration of eosinophils and basophils.

Inhibition of NF- κ B activation by periostin disruption in keratinocytes of FADS mice

It remains undetermined how the disruption of *Ik2* in fibroblasts leads to the appearance of phenotypes similar to patients with AD in FADS mice. To understand the biological effects induced by genetic deficiency of *Ik2* in fibroblasts and the inhibitory effects by periostin disruption *in vivo*, we

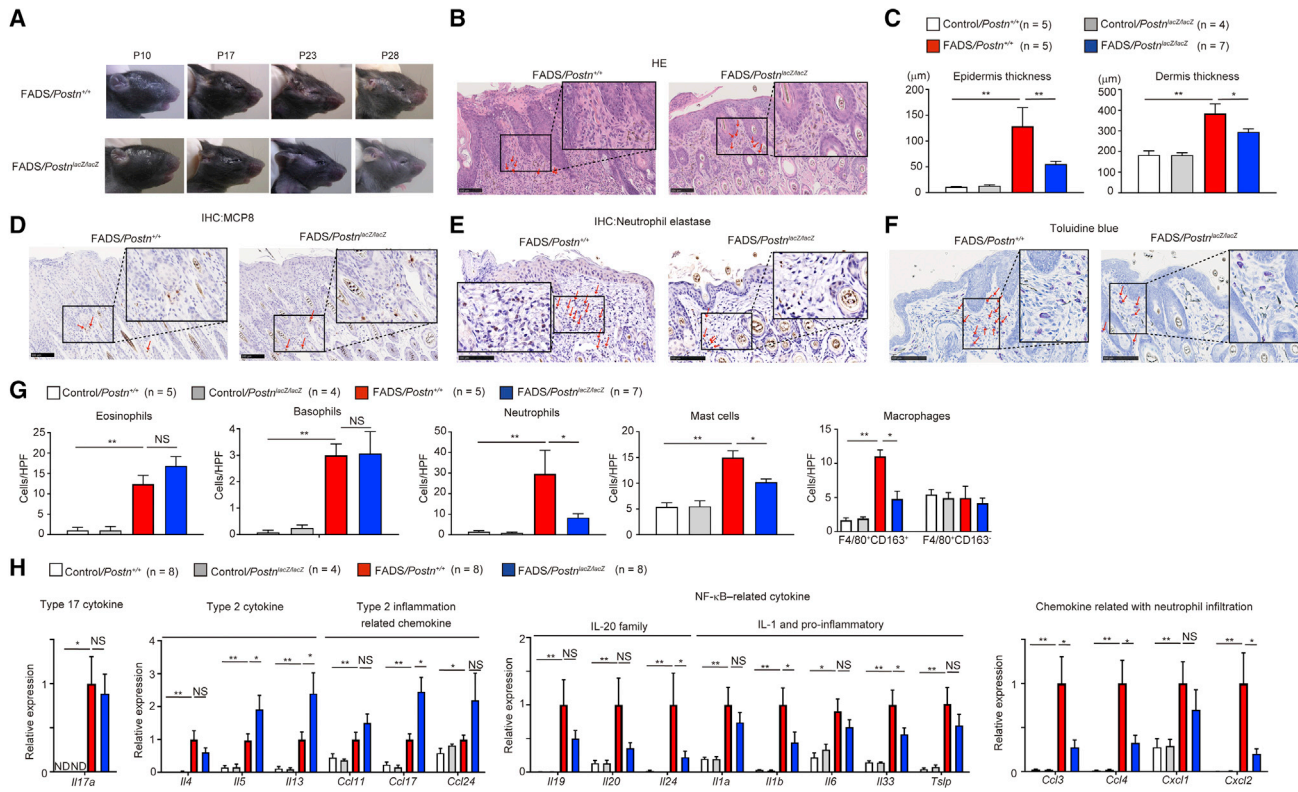


Figure 3. Improved progression of skin inflammation by genetic disruption of periostin in FADS mice

(A) Macroscopic facial skin lesions of FADS/*Postn*^{lacZ/lacZ} mice and FADS/*Postn*^{+/+} mice at the indicated periods after birth (see also Figures S1 and S2). Histological analysis of the facial skin of 4-week-old FADS/*Postn*^{lacZ/lacZ} mice and FADS/*Postn*^{+/+} mice. (B–F) Hematoxylin and eosin staining (B), epidermal and dermal thickness (C), mast cell protease 8 (MCP8) staining (D), neutrophil elastase staining (E), and toluidine blue staining (F) of 4-week-old control/*Postn*^{+/+} mice (n = 5), control/*Postn*^{lacZ/lacZ} mice (n = 4), FADS/*Postn*^{+/+} mice (n = 5), and FADS/*Postn*^{lacZ/lacZ} mice (n = 7). Red arrows indicate eosinophils (B), basophils (D), neutrophils (E) or mast cells (F). Scale bars, 100 μm. (G and H) The number per high-power field (HPF; ×40) of eosinophils, basophils, neutrophils, mast cells, and F4/80⁺CD163⁺ macrophages (G), quantitative real-time PCR analysis for cytokines and chemokines (H) of 4-week-old control/*Postn*^{+/+} mice (n = 8), control/*Postn*^{lacZ/lacZ} mice (n = 4), FADS/*Postn*^{+/+} mice (n = 8), and FADS/*Postn*^{lacZ/lacZ} mice (n = 8). In H, the relative gene expression levels were normalized to *Gapdh*. The mean expression levels for the facial skin of FADS/*Postn*^{+/+} mice are displayed as 1. The data shown are the mean ± standard error of the mean of samples obtained from three (C and G) or four (H) independent experiments. Statistical analysis was performed using a one-sided Mann-Whitney *U*-test; **p* < 0.05, ***p* < 0.01. NS, not significant. IHC, immunohistochemistry.

comprehensively identified the genes that are upregulated in facial skins of FADS mice and are downregulated by periostin disruption using the cap analysis of gene expression (CAGE) method (Table S1 and Figure 4). Comparisons of either the upregulated or downregulated genes in FADS/*Postn*^{+/+} mice compared with control/*Postn*^{+/+} mice and either the upregulated or downregulated genes in FADS/*Postn*^{lacZ/lacZ} mice compared with FADS/*Postn*^{+/+} mice are depicted in the vertical and horizontal axes, respectively (Figure 4A). The cytokines and chemokines that we found were upregulated in FADS/*Postn*^{+/+} mice and were downregulated in FADS/*Postn*^{lacZ/lacZ} mice shown in Figure 4—*Il1b*, *Il24*, *Il33*, *Ccl3*, *Ccl4*, and *Cxcl2* genes—were distributed in the upper left quadrant, indicating concordance between the CAGE method and the quantitative PCR method. We focused on 365 genes in the black square (Table S2) in the upper left quadrant as the genes upregulated in FADS mice and downregulated by periostin disruption, applying these genes to pathway enrichment analysis to characterize them.

Gene ontology analysis showed that genes annotated with keratinization and neutrophil chemotaxis were significantly enriched in the 365 genes (Figure 4B and Table S3), consistent with the histological findings that epidermal hyperplasia and neutrophil infiltration were reduced in FADS/*Postn*^{lacZ/lacZ} mice, as shown in Figure 3. We next examined the transcription factors regulating the genes that are upregulated in FADS mice and are downregulated by periostin disruption. Downstream molecules of NF-κB1 and RelA were enriched in the 365 genes (Figure 4C), and these genes largely involved the genes related to neutrophil chemotaxis, immune response, keratinization and keratinocyte differentiation, and leukocyte activation (Figure 4D). Moreover, NF-κB1 target genes were included in the RelA-target genes (Figure 4E).

These results indicated the possibility that NF-κB molecules are activated in some cells other than nestin-expressing fibroblasts in which *Ikk2*, the critical molecule for the canonical pathway of the NF-κB signals, is deleted, and that periostin is critical in activating these NF-κB molecules. We confirmed that

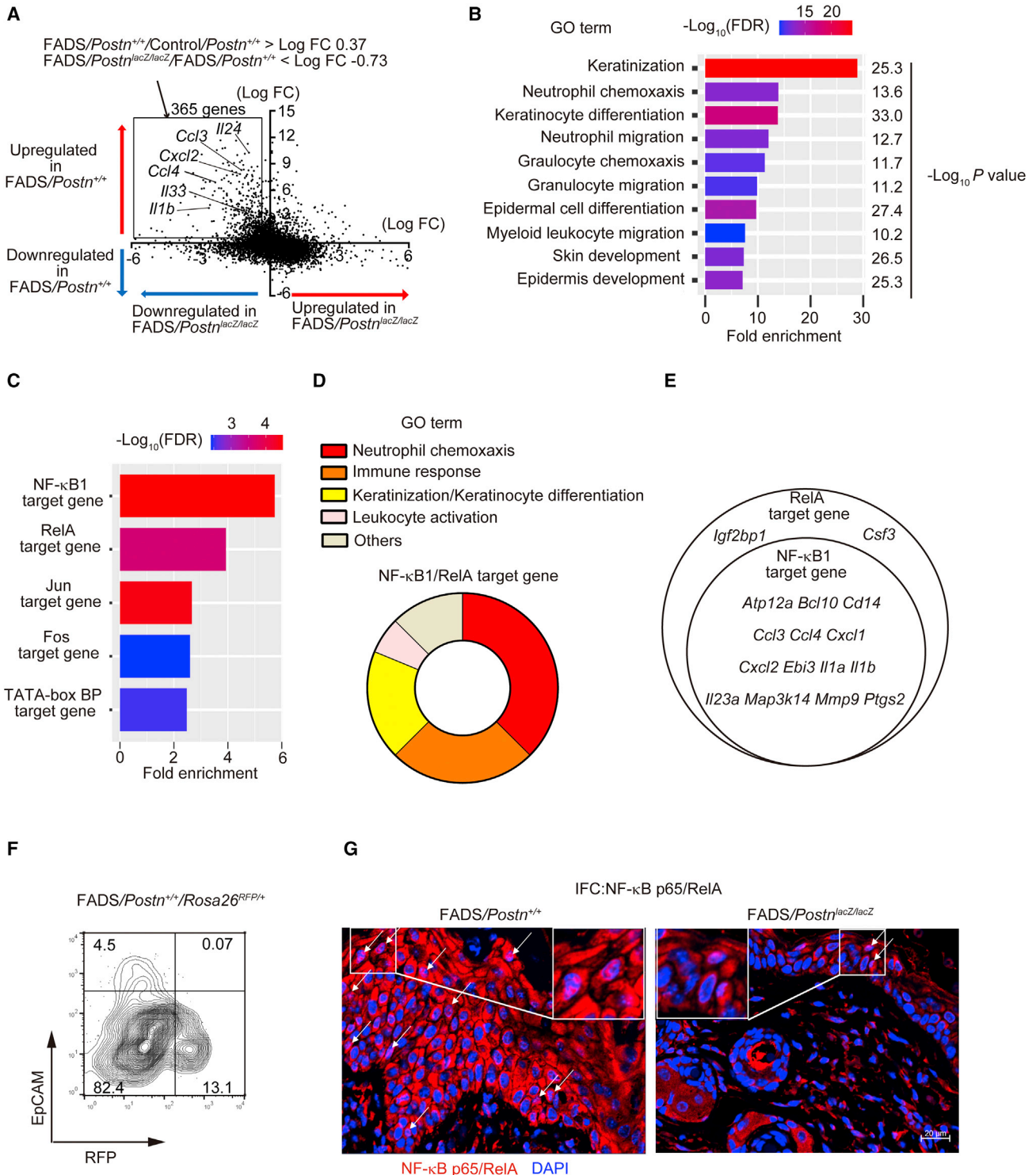


Figure 4. Inhibiting activated NF- κ B pathways in keratinocytes of FADS mice by disrupting periostin

(A) A gene plot of either the upregulated or downregulated genes in facial skins of 4-week-old FADS mice (vertical axis) and either the upregulated or downregulated genes by *Postn* disruption in 4-week-old FADS mice (horizontal axis; see also Table S1). The vertical axis represents the average \log_2 fold-change (FC) of differentially expressed genes between FADS/*Postn*^{+/+} and Control/*Postn*^{+/+} facial skin. The horizontal axis represents the average \log_2 FC of differentially expressed genes between FADS/*Postn*^{lacZ/lacZ} and FADS/*Postn*^{+/+} facial skin, respectively. The 365 genes including representative genes (*Ccl3*, *Ccl4*, *Cxcl2*, *Il1b*, *Il24*, and *Il33*) are depicted in the black square (see also Table S2).

(legend continued on next page)

Ikk2 was expressed in keratinocytes because only a small population expressing both EpCAM⁺ and REFP⁺ existed in FADS/*Postn*^{+/+}/*Rosa26*^{RFPI/+} mice (Figure 4F). We next examined activation of NF-κB p65/Rel A in inflamed skin in FADS/*Postn*^{+/+} and FADS/*Postn*^{lacZ/lacZ} mice. Keratinocytes showed cytosolic expression and nuclear localization of p65, which were diminished in FADS/*Postn*^{lacZ/lacZ} mice (Figure 4G). Taking these results together, NF-κB molecules are spontaneously activated in keratinocytes of FADS mice, and periostin is critical for activating NF-κB molecules in keratinocytes.

Periostin promotes itching by spontaneously firing neurons in FADS mice

We have previously shown that FADS mice spontaneously exhibit severe scratching behaviors because of itching.³⁰ Surprisingly, genetic disruption of periostin significantly decreased scratching behaviors during all of the observed periods from 4 to 12 weeks (Figure 5A and Video S1), suggesting the importance of periostin in causing itching, although it was unclear whether, in FADS mice, the roles of periostin in itching are direct or indirect. We excluded the possibility that decreased scratch behavior was due to decreased motor activities because there was no difference in motor activities between FADS/*Postn*^{+/+} and FADS/*Postn*^{lacZ/lacZ} mice (Figure S3).

We next performed *in vivo* extracellular recording, sensing the firing of superficial dorsal horn neurons (<100 μm from the surface) that receive itch signals from peripheral sensory neurons. We confirmed that recorded neurons were located in dorsal horn at comparable depths in FADS/*Postn*^{+/+} and FADS/*Postn*^{lacZ/lacZ} mice (FADS/*Postn*^{+/+}, 51.2 ± 3.2 μm; FADS/*Postn*^{lacZ/lacZ} 57.3 ± 2.8 μm, Figure S4). The spontaneous firing in the dorsal horn neurons was much higher in FADS/*Postn*^{+/+} mice than in FADS/*Postn*^{lacZ/lacZ} mice (Figure 5B). Scratching bouts and spontaneous firing in FADS/*Postn*^{+/+} and FADS/*Postn*^{lacZ/lacZ} mice showed significant correlations (Figure 5C) (FADS/*Postn*^{+/+}: $r = 0.88$, $p < 0.05$; FADS/*Postn*^{lacZ/lacZ}: $r = 0.96$, $p < 0.01$). These data suggest that periostin promotes itching in FADS mice and increasing spontaneous firing in the dorsal horn neurons would be one of its underlying mechanisms.

Effects of pharmacological inhibition of periostin on skin inflammation and itching in FADS mice

We have previously shown that CP4715, an α_vβ₃ integrin inhibitor, potently inhibits the binding of periostin to the receptor and that administration of CP4715 into mice improves bleomycin-induced lung fibrosis.³⁵ We examined the effects of CP4715 administration into FADS mice on skin inflammation and itching by applying two kinds of administrations: continuous administration (Figure 6A) and single shot. Continuous administration of CP4715 improved eczema (Figure 6B), epidermal thickness (Figures 6C

and 6D), infiltration of neutrophils, mast cells, and M2 macrophages (Figures 6C and 6E). It also improved the expression of NF-κB-related cytokines—*Il1a*, *Il1b*, *Il6*, *Il19*, *Il24*, and *Tslp*—and chemokines related to neutrophil migration—*Ccl3*, *Ccl4*, *Cxcl1*, and *Cxcl2* (Figure 6F). Consistent with these observations, CP4715 treatment decreased cytosolic expression and nuclear localization of p65 in keratinocytes in FADS mice (Figure 6G). Moreover, scratching bouts on day 8 and day 15 after CP4715 treatment were significantly decreased (Figure 6H). We next examined the effects of single-shot administration of CP4715 on itching and spontaneous firing of neurons in FADS mice. The single shot immediately started to decrease the spontaneous firing of neurons, its inhibitory effect reaching the maximum at 40 min after administration (Figure 6I). Scratching bouts were immediately decreased after administration, with inhibitory effects continuing for about 40 min as well (Figure 6J and Video S2), indicating that the effects of periostin on sensory neuron cells are probably direct. We confirmed that the same treatment with CP4715 did not decrease motor activity (Figure S5), excluding a possible sedative effect on the anti-itch actions of CP4715. Furthermore, neutralizing anti-periostin Ab (OC-20) significantly decreased scratching bouts in FADS/*Postn*^{+/+} mice as well (Figure S6). These data suggest that periostin probably directly promotes itching and that in FADS mice, pharmacologically inhibiting periostin by continuously administering CP4715 is effective for improving skin inflammation and itching.

DISCUSSION

We previously established FADS mice by selectively deleting *Ikk2* under the control of nestin expression, finding that, soon after birth, FADS mice spontaneously evoke eczema similar to patients with AD, suggesting that FADS mice would be a useful mouse model of AD. Particularly, since it is suggested that dupilumab sometimes fails to improve skin symptoms of the face despite its dramatic effect on the other body parts,³⁶ this model may be useful to discriminate the pathogenesis of skin inflammation in faces and in bodies in AD. However, the underlying mechanism of how selective deletion of *Ikk2* causes such phenotypes had remained unclear.²⁹ We have demonstrated that activation of STAT3 and STAT6 is pronounced in keratinocytes and in immune cells, respectively, reflecting excess production of inflammatory cytokines in FADS mice²⁹; however, this cannot fully explain the pathogenesis of FADS mice. It has been recently reported that selective deletion of *Ikk2* in Prx1⁺ fibroblasts causes skin inflammation in mice in which infiltration of eosinophils, neutrophils, and macrophages is pronounced.³⁷ The phenotypes of these mice are very similar to FADS mice. It was reported that CCL11 is important for the pathogenesis of these mice, based on the finding that neutralization of CCL11 downregulated infiltration of

(B and C) Gene ontology (GO) pathway analysis (B) (see also Table S3), and transcription factor enrichment analysis (C) of the 365 genes. Statistical significance in enrichment was analyzed using Fisher's exact test in (B).

(D) GO terms of the NF-κB1/RelA-target genes identified in (C).

(E) Venn diagram of genes shared between NF-κB1- and RelA-target genes.

(F) Flow cytometric analysis for RFP positive cells in EpCAM⁺ and EpCAM⁺ facial dermal cells of 4-week-old FADS/*Postn*^{+/+}/*Rosa26*^{RFPI/+} mice.

(G) NF-κB p65 expression in facial skin of 4-week-old FADS/*Postn*^{+/+} mice and FADS/*Postn*^{lacZ/lacZ} mice. Similar results were obtained from three separate experiments. White arrows indicate epidermal cells with nuclear p65 expression. Scale bar, 20 μm.

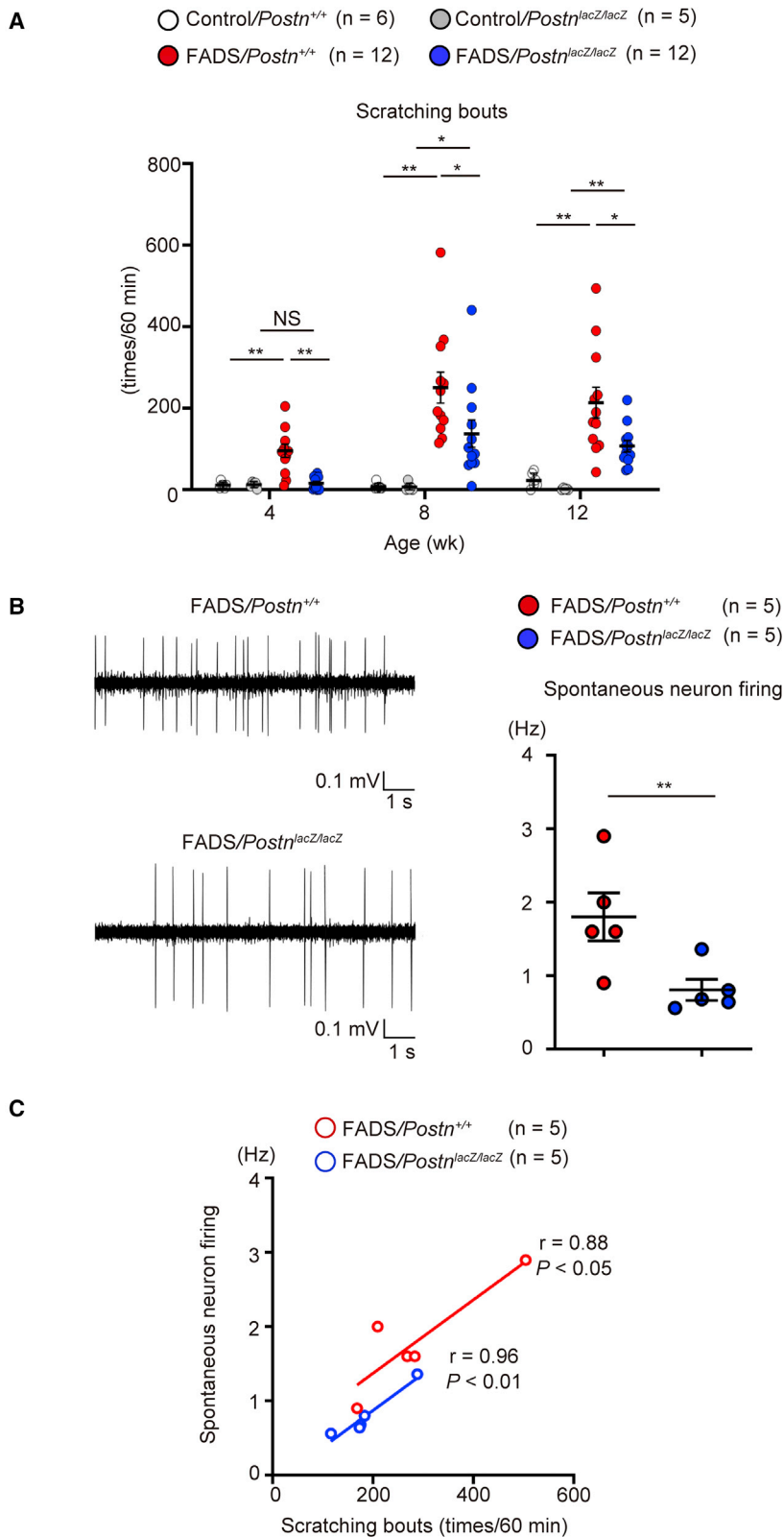


Figure 5. Periostin promotes itching and spontaneous neuron firing in FADS mice

(A) Scratching bouts in control/*Postn*^{+/+} mice (n = 6), control/*Postn*^{lacZ/lacZ} mice (n = 5), FADS/*Postn*^{+/+} mice (n = 12), and FADS/*Postn*^{lacZ/lacZ} mice (n = 12) at the indicated periods after birth.

(B and C) Representative traces (left) and quantitative analysis (right) of spontaneous neuronal firing (B) (see also Figure S4) and correlation between scratching bouts and neuronal firing (C) in 8-week-old FADS/*Postn*^{+/+} mice (n = 5) and FADS/*Postn*^{lacZ/lacZ} mice (n = 5). The data shown are the mean \pm standard error of the mean of samples obtained from five (A) or seven (B and C) independent experiments. Statistical analysis was performed using a one-sided Mann-Whitney *U* test (A–C); **p* < 0.05, ***p* < 0.01. NS, not significant.

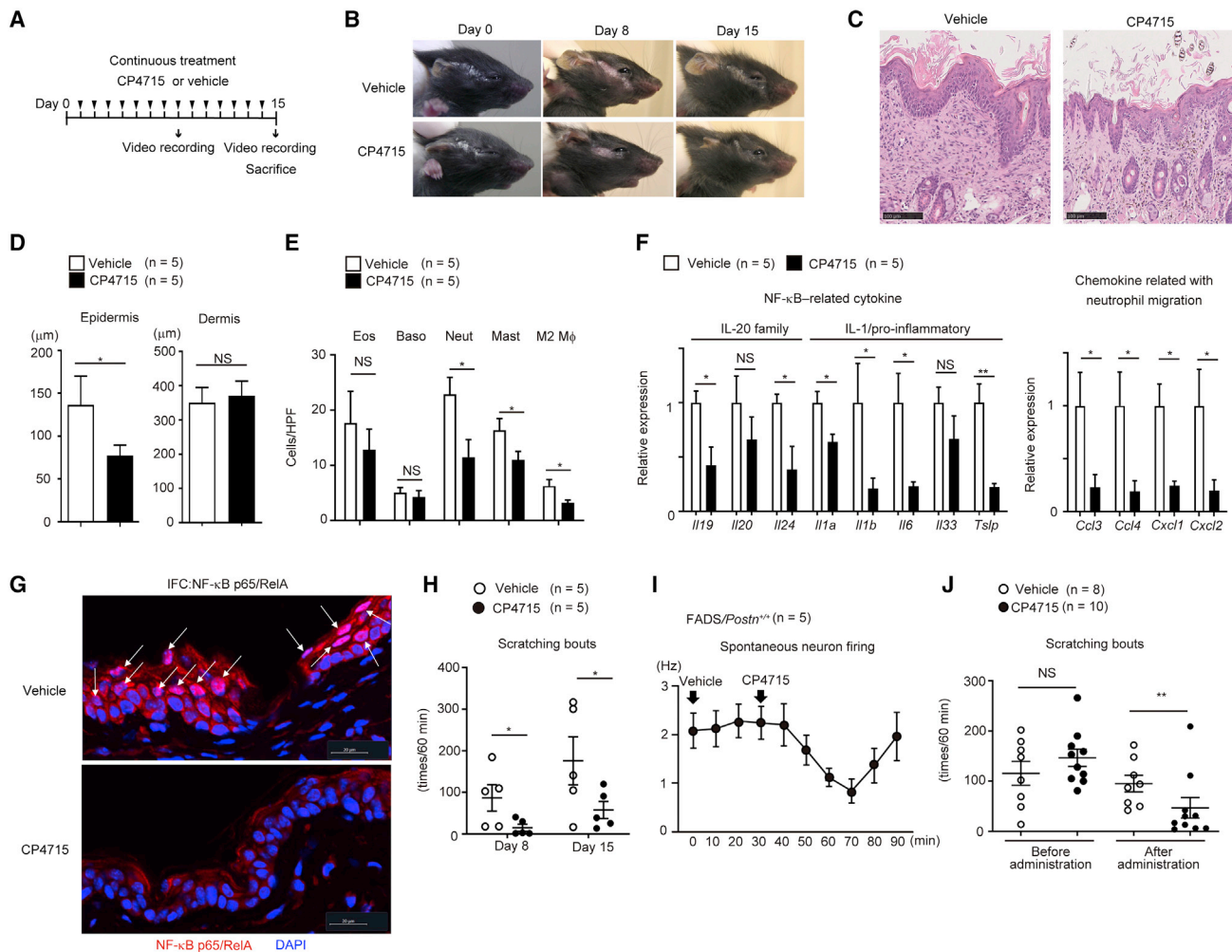


Figure 6. Effects of pharmacologically inhibiting periostin on skin inflammation and itching in FADS mice

(A) The experimental protocol of continuous CP4715 administration.

(B–H) Macroscopic facial skin lesions (B), hematoxylin and eosin staining (C), epidermal and dermal thickness (D), the numbers of per high-power field (HPF; $\times 40$) of the indicated inflammatory cells, expression of the indicated cytokines and chemokines (F), p65 immunostaining (G), and scratching bouts (H) of 3-week-old FADS/Postn^{+/+} mice treated with continuous administration of vehicle (n = 5) or CP4715 (60 mg/kg) (n = 5) on day 0, day 8, and day 15 (B), or on day 15 (C–G), or on day 8 and day 15 (H). Scale bars, 20 (G) or 100 μ m (A). White arrows indicate epidermal cells with nuclear p65 expression (G).

(I and J) Spontaneous firing of dorsal horn neurons (I) and scratching bouts (J) in 60 min after 10- to 14-week-old (I) (n = 5) or 4-week-old (vehicle, n = 8; CP4715, n = 10). (J) FADS/Postn^{+/+} mice were treated with single-shot administration of vehicle or CP4715 (30 mg/kg, see also Figures S5 and S6). The data shown are the mean \pm standard error of the mean of samples obtained from three (D–G), five (I), or four (J) independent experiments. Statistical analysis was performed using a one-sided Mann-Whitney U test; *p < 0.05, **p < 0.01. NS, not significant.

eosinophils and T_H2 cells.³⁷ However, in this study, we show that disrupting or inhibiting periostin did not downregulate CCL11 expression, while many pathological features of FADS mice disappeared after these manipulations (Figure 3H). Alternatively, in this study, we showed that NF- κ B molecules were spontaneously activated in keratinocytes of FADS mice and that inhibiting periostin downregulated activation of NF- κ B molecules together with decreasing expression of NF- κ B-related molecules. These results suggest that the pathological pathways via CCL11 and periostin co-exist in these two kinds of Ikk2-deleted mice. In contrast, we exclude the possibility that the deletion of Ikk2 directly programs expression of periostin in fibroblasts because

nestin-expressing and periostin-producing fibroblasts did not overlap with each other (Figure 2). Considering our results together, we have concluded that the paradoxical, spontaneous activation of NF- κ B molecules in keratinocytes is an important underlying mechanism of FADS mouse and that periostin is critical for the activation.

We have previously demonstrated that, using a three-dimensional organotypic coculture system composed of keratinocytes and fibroblasts, periostin secreted from fibroblasts acts on keratinocytes via its receptors, integrins, activating NF- κ B molecules in keratinocytes.^{23,26} FADS mice spontaneously produce excess amounts of periostin due to enhanced type 2

inflammation, as we previously showed.²⁹ In this study, we showed that fibroblasts, and to a lesser extent keratinocytes, were periostin-producing cells in FADS mice (Figure 2). These results suggest that periostin derived from fibroblasts, and to a lesser extent from keratinocytes, acts on keratinocytes in a paracrine or autocrine manner *in vivo*, as we showed in an *in vitro* system. Subsequent to the previous study, we assumed that the amplification of type 2 inflammation would be a main effect of periostin on NF- κ B activation in keratinocytes, based on the finding that TSLP expression is enhanced in keratinocytes of the three-dimensional organotypic coculture system.^{23,26} However, it turned out in this study that activation of NF- κ B-mediated inflammation, a non-type 2 inflammation, rather than the amplification of type 2 inflammation, would be the main effect of NF- κ B activation in keratinocytes by periostin *in vivo*.

In this study, we showed that, after the activation of NF- κ B in keratinocytes, periostin induced expression of NF- κ B-related cytokines—*Il19*, *Il20*, and *Il24* (IL-20 family cytokines), *Il1a*, *Il1b*, *Il6*, *Il33*, and *Tslp* (IL-1 and pro-inflammatory cytokines)—and *Ccl3*, *Ccl4*, *Cxcl1*, and *Cxcl2* (chemokines related to neutrophil migration, Figures 3 and 6), and keratinization-related molecules (Figure 4), resulting in the infiltration of neutrophils and M2 macrophages, as well as in epidermal hyperplasia (Figures 1 and 3). It is known that IL-4 and IL-13 potentially induce polarization to M2 macrophages.³⁸ In contrast, it has been previously reported that periostin directly promotes polarization to M2 macrophages and recruitment of M2 macrophages.^{39,40} Therefore, periostin may be involved in the infiltration of M2 macrophages by either enhancing M2 polarization or recruitment of M2 macrophages, independent of IL-4 and IL-13. Although it is known that neutrophilia is correlated with the clinical severity of AD in patients, its precise pathological significance remains undetermined.^{41,42} It has been reported that neutrophils increase colonization of *Staphylococcus aureus*, a potent pathogen for patients with AD, and that neutrophils promote chronic itching via CXCL10 production.^{43,44} In accord with these findings, a recent study demonstrated that the blockade of neutrophil infiltration by anti-CXCR2 Ab abrogates acanthosis with spongiosis, parakeratosis, and itch in allergic skin inflammation.⁴⁵ Massive infiltration of M2 macrophages is a typical feature of chronic AD skin.^{46,47} Since M2 macrophages have the potential to produce pro-fibrogenic mediators, M2 macrophages are thought to be involved in dermal fibrosis in chronic AD.⁴⁸ Epidermal hyperplasia contributing to formation of hyper- and parakeratosis is also known to be a typical feature of AD and is correlated with clinical severity.^{49–51} Although the precise significance of epidermal hyperplasia in the pathogenesis of AD remains unclear, it has been reported that epidermal hyperplasia decreases sweating in patients with AD, thereby exacerbating skin inflammation and itching.^{52,53} Moreover, we have proposed that epidermal hyperplasia may contribute to massive production of pro-inflammatory cytokines from keratinocytes.²³ In accordance with these presumed functions of neutrophil infiltration, M2 macrophage infiltration, and epidermal hyperplasia, it is known that activation of NF- κ B molecules in keratinocytes is a characteristic of severe AD in patients.⁵⁴ These results indicate that the FADS mouse is a model similar to severe AD in patients and that periostin

is involved in exacerbation of skin inflammation of AD by linking NF- κ B-related inflammation with type 2 inflammation.

Linkage between type 2 inflammation and itching has recently been proposed: type 2 cytokines—IL-4, IL-13, IL-31, IL-33, and TSLP—act on mouse NP2 and NP3 type neurons, followed by the activation of TRPV1 and/or TRPA1, evoking itching.^{15,17–20} But the expression of IL-4 and IL-13 was not downregulated in periostin-inhibited FADS mice, while itching was significantly decreased in these mice (Figures 3H and 5A). Moreover, as we previously showed, IL-31 expression was not increased in FADS mice²⁹ and neither genetic disruption nor pharmacological inhibition of periostin changed IL-31 expression (Figure S7). These results suggest that neither IL-4, IL-13, nor IL-31 might be involved in itching in FADS mice. Since either genetic disruption or pharmacological inhibition of periostin downregulated recruitment of neutrophils, but not expression of CXCL10 (Figure S7), it is unlikely in FADS mouse that the neutrophil-CXCL10-CXCR3 pathway is involved in promoting itching, as previously suggested.⁴⁴ In contrast, genetic disruption or pharmacological inhibition of periostin significantly decreased itching in FADS mice (Figures 5 and 6). Of particular importance is that single-shot administration of CP4715 immediately started to downregulate spontaneous neuron firing, followed by decreased scratching behaviors (Figures 6I and 6J). These results strongly suggest that periostin directly acts on sensory neurons, evoking itching. Mishra et al.²⁷ have reported that, by administering periostin into several animals and using a neurophysiological approach, periostin directly activates DRG sensory neurons, inducing itching. Moreover, they showed that conditional disruption of β 3 integrin on nerve cells decreased MC903-induced itching. Our present findings support their observations. Alternatively, it is known that several epithelial cytokines such as IL-33 and TSLP directly activate peripheral sensory neurons followed by the activation of TRPV1 and/or TRPA1, evoking itching¹⁶ and either genetic disruption or continuous pharmacological inhibition of periostin decrease the expression of IL-33 and/or TSLP in the facial skin of FADS mice (Figures 3, 4, and 6). Therefore, it is also possible that periostin indirectly promotes itching via production of IL-33 and TSLP. The underlying mechanism of how type 2 inflammation causes itching may be heterogeneous.^{12,16} It is of note that the effect of genetic disruption on itching is more obvious in 4-week-old FADS mice than in older ones (Figure 5A), suggesting that the contribution of periostin to itching may be different among the stages of skin inflammation. We need to clarify this point for patients with AD in the future.

In this study, we showed that the genetic disruption of periostin did not prevent the onset, but rather the development, of skin inflammation (Figures 3A and S2), suggesting that genetic inhibition of periostin would be useful for ameliorating rather than preventing allergic skin inflammation. In accordance with this notion, CP4715, an inhibitor against $\alpha_v\beta_3$ integrin, improved skin inflammation together with itching in FADS mice (Figure 6). CP4715 is a low-molecular compound having a tetrahydropyrimidin-2-yl-amino moiety at the N-terminus and a benzoyl moiety at the center and was developed as an integrin inhibitor.^{55–58} We confirmed that CP4715 has a potent inhibitory effect on the interaction between periostin and $\alpha_v\beta_3$ integrin and that administering CP4715 improved bleomycin-induced lung fibrosis in mice by

blocking the periostin signals.³⁵ Mishra et al.²⁷ demonstrated the inhibitory effects of cilengitide, another inhibitor against $\alpha_v\beta_3/\alpha_v\beta_5$, on activation of DRG sensory neurons by periostin. These results suggest that the interaction between periostin and $\alpha_v\beta_3$ would be a promising therapeutic target for the treating patients with AD, particularly for itching. Given that the underlying mechanism of itching is heterogeneous among patients with AD, it is hoped that a therapeutic agent targeting this interaction will be developed to realize precision medicine for AD.

Limitations of the study

It remains unclear which subtype of patients with AD show the same pathogenesis of skin inflammation and itching as that of FADS mouse, because it is thought that the pathogenesis of AD is heterogeneous.^{8,12,16} It is awaited to stratify the endotypes of AD more clearly and to investigate which endotype of AD corresponds with the pathogenesis of FADS mouse. Unfortunately, the present study was not designed to analyze clinical samples from patients with AD. Thus, we could not examine the relationship between expression levels of periostin in skin lesions and in blood and the severity of itching in different endotypes of AD. Moreover, we examined the effects of periostin deficiency or inhibition mainly on skin tissues in this study. It is important to analyze the effects of periostin deficiency or inhibition on non-skin tissues such as the nerve system in the future. In this study, we focused on periostin as a pruritogen. However, it is known that various type 2 cytokines also acts as pruritogens. We need to clarify specificity and/or redundancy of these type 2 mediators as pruritogens in the future.

STAR★METHODS

Detailed methods are provided in the online version of this paper and include the following:

- KEY RESOURCES TABLE
- RESOURCE AVAILABILITY
 - Lead contact
 - Materials availability
 - Data and code availability
- EXPERIMENTAL MODEL AND SUBJECT DETAILS
 - Animals
 - Preparation of primary dermal fibroblasts and dermal cells
- METHOD DETAILS
 - Flow cytometry
 - Immunohistochemistry and special stains
 - Immunofluorescence detection by confocal microscopy
 - Quantitative real-time PCR
 - Cap Analysis of Gene Expression (CAGE)
 - Monitoring of scratching behavior
 - Drug treatment
 - Measurement of motor activity
 - *In vivo* extracellular recording from superficial dorsal horn neurons
- QUANTIFICATION AND STATISTICAL ANALYSIS

SUPPLEMENTAL INFORMATION

Supplemental information can be found online at <https://doi.org/10.1016/j.celrep.2022.111933>.

ACKNOWLEDGMENTS

The authors thank Dr. Dovie R. Wylie for the critical review of this manuscript. We also thank Ms. Maki Watanabe and Ms. Tomoyo Yoshida for their technical assistance. We thank Dr. Manolis Pasparakis, Dr. Gail R. Martin, and Dr. Hans Joerg Fehling for their kindness in providing *Ikk2^{fl/fl}*, *Nestin^{Cre}*, and *Rosa26^{RFPP}* mice. We thank Mr. Koukichi Suzuki (Meiji Seika Pharma) for providing CP4715. We also thank Ms. Eno Nakano and Mr. Ryunosuke Nishizawa for helping with the analyses. This work was supported in part by JSPS KAKENHI Grant Number #JP16H05343 (to K.I.) and #JP19K08912 (to S.N.).

AUTHOR CONTRIBUTIONS

Conceptualization, S.N., Y.N., I.K., and K.I.; Methodology, S.N., D.U., and K.M.; Investigation, S.N., D.U., I.K., K.M., H.I., N.E., M. Kitajima, M. Koga, S.Y., Y.H., H.T. and T.A.; Writing – Original Draft, S.N., Y.N., D.U., T.A., I.K., and K.I.; Funding Acquisition, S.N., and K.I.; Resources, S.J.C.; Supervision, S.J.C., I.K., and K.I.

DECLARATION OF INTERESTS

The authors declare no competing financial interest.

Received: August 15, 2022

Revised: November 6, 2022

Accepted: December 15, 2022

REFERENCES

1. Furue, M., Chiba, T., Tsuji, G., Ulzii, D., Kido-Nakahara, M., Nakahara, T., and Kadono, T. (2017). Atopic dermatitis: immune deviation, barrier dysfunction, IgE autoreactivity and new therapies. *Allergol. Int.* 66, 398–403. <https://doi.org/10.1016/j.alit.2016.12.002>.
2. Bieber, T. (2020). Interleukin-13: targeting an underestimated cytokine in atopic dermatitis. *Allergy* 75, 54–62. <https://doi.org/10.1111/all.13954>.
3. Blauvelt, A., de Bruin-Weller, M., Gooderham, M., Cather, J.C., Weisman, J., Pariser, D., Simpson, E.L., Papp, K.A., Hong, H.C.H., Rubel, D., et al. (2017). Long-term management of moderate-to-severe atopic dermatitis with dupilumab and concomitant topical corticosteroids (LIBERTY AD CHRONOS): a 1-year, randomised, double-blinded, placebo-controlled, phase 3 trial. *Lancet* 389, 2287–2303. [https://doi.org/10.1016/S0140-6736\(17\)31191-1](https://doi.org/10.1016/S0140-6736(17)31191-1).
4. Esaki, H., Brunner, P.M., Renert-Yuval, Y., Czarnowicki, T., Huynh, T., Tran, G., Lyon, S., Rodriguez, G., Immaneni, S., Johnson, D.B., et al. (2016). Early-onset pediatric atopic dermatitis is Th2 but also Th17 polarized in skin. *J. Allergy Clin. Immunol.* 138, 1639–1651. <https://doi.org/10.1016/j.jaci.2016.07.013>.
5. Gittler, J.K., Shemer, A., Suárez-Fariñas, M., Fuentes-Duculan, J., Gulewicz, K.J., Wang, C.Q.F., Mitsui, H., Cardinale, I., de Guzman Strong, C., Krueger, J.G., and Guttman-Yassky, E. (2012). Progressive activation of T(H)2/T(H)22 cytokines and selective epidermal proteins characterizes acute and chronic atopic dermatitis. *J. Allergy Clin. Immunol.* 130, 1344–1354. <https://doi.org/10.1016/j.jaci.2012.07.012>.
6. Leung, D.Y.M., Boguniewicz, M., Howell, M.D., Nomura, I., and Hamid, Q.A. (2004). New insights into atopic dermatitis. *J. Clin. Invest.* 113, 651–657. <https://doi.org/10.1172/JCI21060>.
7. Möbus, L., Rodriguez, E., Harder, I., Stölz, D., Boraczynski, N., Gerdes, S., Kleinheinz, A., Abraham, S., Heratizadeh, A., Handrick, C., et al. (2021). Atopic dermatitis displays stable and dynamic skin transcriptome

- signatures. *J. Allergy Clin. Immunol.* **147**, 213–223. <https://doi.org/10.1016/j.jaci.2020.06.012>.
8. Czarnowicki, T., He, H., Krueger, J.G., and Guttman-Yassky, E. (2019). Atopic dermatitis endotypes and implications for targeted therapeutics. *J. Allergy Clin. Immunol.* **143**, 1–11. <https://doi.org/10.1016/j.jaci.2018.10.032>.
 9. He, H., Del Duca, E., Diaz, A., Kim, H.J., Gay-Mimbrera, J., Zhang, N., Wu, J., Beaziz, J., Estrada, Y., Krueger, J.G., et al. (2021). Mild atopic dermatitis lacks systemic inflammation and shows reduced nonlesional skin abnormalities. *J. Allergy Clin. Immunol.* **147**, 1369–1380. <https://doi.org/10.1016/j.jaci.2020.08.041>.
 10. Konrad, R.J., Higgs, R.E., Rodgers, G.H., Ming, W., Qian, Y.W., Bivi, N., Mack, J.K., Siegel, R.W., and Nickoloff, B.J. (2019). Assessment and clinical relevance of serum IL-19 levels in psoriasis and atopic dermatitis using a sensitive and specific novel immunoassay. *Sci. Rep.* **9**, 5211. <https://doi.org/10.1038/s41598-019-41609-z>.
 11. Brunner, P.M., Khattri, S., Garocet, S., Finney, R., Oliva, M., Dutt, R., Fuentes-Duculan, J., Zheng, X., Li, X., Bonifacio, K.M., et al. (2016). A mild topical steroid leads to progressive anti-inflammatory effects in the skin of patients with moderate-to-severe atopic dermatitis. *J. Allergy Clin. Immunol.* **138**, 169–178. <https://doi.org/10.1016/j.jaci.2015.12.1323>.
 12. Garcovich, S., Maurelli, M., Gisondi, P., Peris, K., Yosipovitch, G., and Girolomoni, G. (2021). Pruritus as a distinctive feature of type 2 inflammation. *Vaccines* **9**, 303. <https://doi.org/10.3390/vaccines9030303>.
 13. Rerknimitr, P., Otsuka, A., Nakashima, C., and Kabashima, K. (2017). The etiopathogenesis of atopic dermatitis: barrier disruption, immunological derangement, and pruritus. *Inflamm. Regen.* **37**, 14. <https://doi.org/10.1186/s41232-017-0044-7>.
 14. Cevikbas, F., and Lerner, E.A. (2020). Physiology and pathophysiology of itch. *Physiol. Rev.* **100**, 945–982. <https://doi.org/10.1152/physrev.00017.2019>.
 15. Dong, X., and Dong, X. (2018). Peripheral and central mechanisms of itch. *Neuron* **98**, 482–494. <https://doi.org/10.1016/j.neuron.2018.03.023>.
 16. Wang, F., and Kim, B.S. (2020). Itch: a paradigm of neuroimmune crosstalk. *Immunity* **52**, 753–766. <https://doi.org/10.1016/j.immuni.2020.04.008>.
 17. Feld, M., Garcia, R., Buddenkotte, J., Katayama, S., Lewis, K., Muirhead, G., Hevezi, P., Plessner, K., Schrupf, H., Krjutskov, K., et al. (2016). The pruritus- and TH2-associated cytokine IL-31 promotes growth of sensory nerves. *J. Allergy Clin. Immunol.* **138**, 500–508.e24. <https://doi.org/10.1016/j.jaci.2016.02.020>.
 18. Liu, B., Tai, Y., Achanta, S., Kaelberer, M.M., Caceres, A.I., Shao, X., Fang, J., and Jordt, S.E. (2016). IL-33/ST2 signaling excites sensory neurons and mediates itch response in a mouse model of poison ivy contact allergy. *Proc. Natl. Acad. Sci. USA* **113**, E7572–E7579. <https://doi.org/10.1073/pnas.1606608113>.
 19. Moran, T.P., and Vickery, B.P. (2014). The epithelial cell-derived atopic dermatitis cytokine TSLP activates neurons to induce itch. *Pediatrics* **134**, S160–S161. <https://doi.org/10.1542/peds.2014-1817V>.
 20. Oetjen, L.K., Mack, M.R., Feng, J., Whelan, T.M., Niu, H., Guo, C.J., Chen, S., Trier, A.M., Xu, A.Z., Tripathi, S.V., et al. (2017). Sensory neurons co-opt classical immune signaling pathways to mediate chronic itch. *Cell* **171**, 217–228.e13. <https://doi.org/10.1016/j.cell.2017.08.006>.
 21. Conway, S.J., Izuhara, K., Kudo, Y., Litvin, J., Markwald, R., Ouyang, G., Arron, J.R., Holweg, C.T.J., and Kudo, A. (2014). The role of periostin in tissue remodeling across health and disease. *Cell. Mol. Life Sci.* **71**, 1279–1288. <https://doi.org/10.1007/s00018-013-1494-y>.
 22. Izuhara, K., Nunomura, S., Nanri, Y., Ono, J., Takai, M., and Kawaguchi, A. (2019). Periostin: an emerging biomarker for allergic diseases. *Allergy* **74**, 2116–2128. <https://doi.org/10.1111/all.13814>.
 23. Masuoka, M., Shiraiishi, H., Ohta, S., Suzuki, S., Arima, K., Aoki, S., Toda, S., Inagaki, N., Kurihara, Y., Hayashida, S., et al. (2012). Periostin promotes chronic allergic inflammation in response to Th2 cytokines. *J. Clin. Invest.* **122**, 2590–2600. <https://doi.org/10.1172/JCI58978>.
 24. Takayama, G., Arima, K., Kanaji, T., Toda, S., Tanaka, H., Shoji, S., McKenzie, A.N.J., Nagai, H., Hotokebuchi, T., and Izuhara, K. (2006). Periostin: a novel component of subepithelial fibrosis of bronchial asthma downstream of IL-4 and IL-13 signals. *J. Allergy Clin. Immunol.* **118**, 98–104. <https://doi.org/10.1016/j.jaci.2006.02.046>.
 25. Kou, K., Okawa, T., Yamaguchi, Y., Ono, J., Inoue, Y., Kohno, M., Matsukura, S., Kambara, T., Ohta, S., Izuhara, K., and Aihara, M. (2014). Periostin levels correlate with disease severity and chronicity in patients with atopic dermatitis. *Br. J. Dermatol.* **171**, 283–291. <https://doi.org/10.1111/bjd.12943>.
 26. Shiraiishi, H., Masuoka, M., Ohta, S., Suzuki, S., Arima, K., Taniguchi, K., Aoki, S., Toda, S., Yoshimoto, T., Inagaki, N., et al. (2012). Periostin contributes to the pathogenesis of atopic dermatitis by inducing TSLP production from keratinocytes. *Allergol. Int.* **61**, 563–572. <https://doi.org/10.2332/allergolint.10-OA-0297>.
 27. Mishra, S.K., Wheeler, J.J., Pitake, S., Ding, H., Jiang, C., Fukuyama, T., Paps, J.S., Ralph, P., Coyne, J., Parkington, M., et al. (2020). Periostin activation of integrin receptors on sensory neurons induces allergic itch. *Cell Rep.* **31**, 107472. <https://doi.org/10.1016/j.celrep.2020.03.036>.
 28. Hashimoto, T., Nattkemper, L.A., Kim, H.S., Kursewicz, C.D., Fowler, E., Shah, S.M., Nanda, S., Fayne, R.A., Romanelli, P., and Yosipovitch, G. (2021). Dermal periostin: a new player in itch of prurigo nodularis. *Acta Derm. Venereol.* **101**, adv00375. <https://doi.org/10.2340/00015555-3702>.
 29. Nunomura, S., Ejiri, N., Kitajima, M., Nanri, Y., Arima, K., Mitamura, Y., Yoshihara, T., Fujii, K., Takao, K., Imura, J., et al. (2019). Establishment of a mouse model of atopic dermatitis by deleting *Ikk2* in dermal fibroblasts. *J. Invest. Dermatol.* **139**, 1274–1283. <https://doi.org/10.1016/j.jid.2018.10.047>.
 30. Nunomura, S., Kitajima, I., Nanri, Y., Kitajima, M., Ejiri, N., Lai, I.S., Okada, N., and Izuhara, K. (2021). The FADS mouse: a novel mouse model of atopic keratoconjunctivitis. *J. Allergy Clin. Immunol.* **148**, 1596–1602.e1. <https://doi.org/10.1016/j.jaci.2021.05.017>.
 31. He, H., Suryawanshi, H., Morozov, P., Gay-Mimbrera, J., Del Duca, E., Kim, H.J., Kameyama, N., Estrada, Y., Der, E., Krueger, J.G., et al. (2020). Single-cell transcriptome analysis of human skin identifies novel fibroblast subpopulation and enrichment of immune subsets in atopic dermatitis. *J. Allergy Clin. Immunol.* **145**, 1615–1628. <https://doi.org/10.1016/j.jaci.2020.01.042>.
 32. Kim, D.W., Kulka, M., Jo, A., Eun, K.M., Arizmendi, N., Tancowny, B.P., Hong, S.N., Lee, J.P., Jin, H.R., Lockey, R.F., et al. (2017). Cross-talk between human mast cells and epithelial cells by IgE-mediated periostin production in eosinophilic nasal polyps. *J. Allergy Clin. Immunol.* **139**, 1692–1695.e6. <https://doi.org/10.1016/j.jaci.2016.09.026>.
 33. Mitamura, Y., Nunomura, S., Nanri, Y., Ogawa, M., Yoshihara, T., Masuoka, M., Tsujii, G., Nakahara, T., Hashimoto-Hachiya, A., Conway, S.J., et al. (2018). The IL-13/periostin/IL-24 pathway causes epidermal barrier dysfunction in allergic skin inflammation. *Allergy* **73**, 1881–1891. <https://doi.org/10.1111/all.13437>.
 34. Shoda, T., Futamura, K., Kobayashi, F., Saito, H., Matsumoto, K., and Matsuda, A. (2013). Cell type-dependent effects of corticosteroid on periostin production by primary human tissue cells. *Allergy* **68**, 1467–1470. <https://doi.org/10.1111/all.12240>.
 35. Nanri, Y., Nunomura, S., Terasaki, Y., Yoshihara, T., Hirano, Y., Yokosaki, Y., Yamaguchi, Y., Feghali-Bostwick, C., Ajito, K., Murakami, S., et al. (2020). Cross-talk between transforming growth factor- β and periostin can be targeted for pulmonary fibrosis. *Am. J. Respir. Cell Mol. Biol.* **62**, 204–216. <https://doi.org/10.1165/rcmb.2019-0245OC>.
 36. Licata, G., Gambardella, A., Tancredi, V., Calabrese, G., De Rosa, A., Alfano, R., and Argenziano, G. (2022). Face atopic dermatitis resistant to dupilumab: a case series of three patients successfully treated with upadacitinib. *J. Eur. Acad. Dermatol. Venereol.* **36**, e150–e152. <https://doi.org/10.1111/jdv.17705>.
 37. Ko, K.I., Merlet, J.J., DerGarabedian, B.P., Zhen, H., Suzuki-Horiuchi, Y., Hedberg, M.L., Hu, E., Nguyen, A.T., Prouty, S., Alawi, F., et al. (2022). NF- κ B perturbation reveals unique immunomodulatory functions in Prx1+

- fibroblasts that promote development of atopic dermatitis. *Sci. Transl. Med.* *14*, eabj0324. <https://doi.org/10.1126/scitranslmed.abj0324>.
38. Sica, A., and Mantovani, A. (2012). Macrophage plasticity and polarization: in vivo veritas. *J. Clin. Invest.* *122*, 787–795. <https://doi.org/10.1172/JCI59643>.
 39. Zhou, W., Ke, S.Q., Huang, Z., Flavahan, W., Fang, X., Paul, J., Wu, L., Sloan, A.E., McLendon, R.E., Li, X., et al. (2015). Periostin secreted by glioblastoma stem cells recruits M2 tumour-associated macrophages and promotes malignant growth. *Nat. Cell Biol.* *17*, 170–182. <https://doi.org/10.1038/ncb3090>.
 40. Kormann, R., Kavvadas, P., Placier, S., Vandermeersch, S., Dorison, A., Dussaule, J.C., Chadichristos, C.E., Prakoura, N., and Chatziantoniou, C. (2020). Periostin promotes cell proliferation and macrophage polarization to drive repair after AKI. *J. Am. Soc. Nephrol.* *31*, 85–100. <https://doi.org/10.1681/ASN.2019020113>.
 41. Inokuchi-Sakata, S., Ishiui, Y., Katsuta, M., Kharma, B., Yasuda, K.I., Tominaga, M., Takamori, K., Nobeyama, Y., and Asahina, A. (2021). Role of eosinophil relative count and neutrophil-to-lymphocyte ratio in the assessment of severity of atopic dermatitis. *Acta Derm. Venereol.* *101*, adv00491. <https://doi.org/10.2340/00015555-3838>.
 42. Jiang, Y., and Ma, W. (2017). Assessment of neutrophil-to-lymphocyte ratio and platelet-to-lymphocyte ratio in atopic dermatitis patients. *Med. Sci. Monit.* *23*, 1340–1346. <https://doi.org/10.12659/msm.900212>.
 43. Bitschar, K., Staudenmaier, L., Klink, L., Focken, J., Sauer, B., Fehrenbacher, B., Herster, F., Bittner, Z., Bleul, L., Schaller, M., et al. (2020). *Staphylococcus aureus* skin colonization is enhanced by the interaction of neutrophil extracellular traps with keratinocytes. *J. Invest. Dermatol.* *140*, 1054–1065.e4. <https://doi.org/10.1016/j.jid.2019.10.017>.
 44. Walsh, C.M., Hill, R.Z., Schwendinger-Schreck, J., Deguine, J., Brock, E.C., Kucirek, N., Rifi, Z., Wei, J., Gronert, K., Brem, R.B., et al. (2019). Neutrophils promote CXCR3-dependent itch in the development of atopic dermatitis. *Elife* *8*, e48448. <https://doi.org/10.7554/eLife.48448>.
 45. Alam, M.J., Xie, L., Ang, C., Fahimi, F., Willingham, S.B., Kueh, A.J., Herold, M.J., Mackay, C.R., and Robert, R. (2020). Therapeutic blockade of CXCR2 rapidly clears inflammation in arthritis and atopic dermatitis models: demonstration with surrogate and humanized antibodies. *mAbs* *12*, 1856460. <https://doi.org/10.1080/19420862.2020.1856460>.
 46. Kiekens, R.C., Thepen, T., Oosting, A.J., Bihari, I.C., Van De Winkel, J.G., Bruijnzeel-Koomen, C.A., and Knol, E.F. (2001). Heterogeneity within tissue-specific macrophage and dendritic cell populations during cutaneous inflammation in atopic dermatitis. *Br. J. Dermatol.* *145*, 957–965. <https://doi.org/10.1046/j.1365-2133.2001.04508.x>.
 47. Toda, M., Leung, D.Y.M., Molet, S., Boguniewicz, M., Taha, R., Christodoulouopoulos, P., Fukuda, T., Elias, J.A., and Hamid, Q.A. (2003). Polarized in vivo expression of IL-11 and IL-17 between acute and chronic skin lesions. *J. Allergy Clin. Immunol.* *111*, 875–881.
 48. Kasraie, S., and Werfel, T. (2013). Role of macrophages in the pathogenesis of atopic dermatitis. *Mediators Inflamm.* *2013*, 942375. <https://doi.org/10.1155/2013/942375>.
 49. Hanifin, J.M., Thurston, M., Omoto, M., Cherill, R., Tofte, S.J., and Graeber, M. (2001). The eczema area and severity index (EASI): assessment of reliability in atopic dermatitis. EASI Evaluator Group. *Exp. Dermatol.* *10*, 11–18. <https://doi.org/10.1034/j.1600-0625.2001.100102.x>.
 50. Leung, D.Y. (1995). Atopic dermatitis: the skin as a window into the pathogenesis of chronic allergic diseases. *J. Allergy Clin. Immunol.* *96*, 302, quiz 319. [https://doi.org/10.1016/s0091-6749\(95\)70049-8](https://doi.org/10.1016/s0091-6749(95)70049-8).
 51. Noda, S., Suárez-Fariñas, M., Ungar, B., Kim, S.J., de Guzman Strong, C., Xu, H., Peng, X., Estrada, Y.D., Nakajima, S., Honda, T., et al. (2015). The Asian atopic dermatitis phenotype combines features of atopic dermatitis and psoriasis with increased TH17 polarization. *J. Allergy Clin. Immunol.* *136*, 1254–1264. <https://doi.org/10.1016/j.jaci.2015.08.015>.
 52. Murota, H., Yamaga, K., Ono, E., Murayama, N., Yokozeki, H., and Katayama, I. (2019). Why does sweat lead to the development of itch in atopic dermatitis? *Exp. Dermatol.* *28*, 1416–1421. <https://doi.org/10.1111/exd.13981>.
 53. Shindo, S., Murota, H., Seki, T., Mori, K., Kaizu, K., Nishizaka, T., Takagi, Y., and Katayama, I. (2022). Effects of a moisturizer containing pseudo-ceramide and a eucalyptus extract on sweating function in adult atopic dermatitis: a double-blind, randomized, controlled left-right comparison clinical trial. *J. Cosmet. Dermatol.* *21*, 4503–4509. <https://doi.org/10.1111/jocd.14923>.
 54. Wang, Y., Weng, H., Song, J.F., Deng, Y.H., Li, S., and Liu, H.B. (2017). Activation of the HMGB1-TLR4-NF- κ B pathway may occur in patients with atopic eczema. *Mol. Med. Rep.* *16*, 2714–2720. <https://doi.org/10.3892/mmr.2017.6942>.
 55. Ishikawa, M., Kubota, D., Yamamoto, M., Kuroda, C., Iguchi, M., Koyanagi, A., Murakami, S., and Ajito, K. (2006). Tricyclic pharmacophore-based molecules as novel integrin $\alpha(v)\beta3$ antagonists. Part 2: synthesis of potent $\alpha(v)\beta3/\alpha(IIb)\beta3$ dual antagonists. *Bioorg. Med. Chem.* *14*, 2109–2130. <https://doi.org/10.1016/j.bmc.2005.10.061>.
 56. Kubota, D., Ishikawa, M., Yamamoto, M., Murakami, S., Hachisu, M., Katanok, K., and Ajito, K. (2006). Tricyclic pharmacophore-based molecules as novel integrin $\alpha(v)\beta3$ antagonists. Part 1: design and synthesis of a lead compound exhibiting $\alpha(v)\beta3/\alpha(IIb)\beta3$ dual antagonistic activity. *Bioorg. Med. Chem.* *14*, 2089–2108. <https://doi.org/10.1016/j.bmc.2005.10.060>.
 57. Ishikawa, M., Hiraiwa, Y., Kubota, D., Tsumahima, M., Watanabe, T., Murakami, S., Ouchi, S., and Ajito, K. (2006). Tricyclic pharmacophore-based molecules as novel integrin $\alpha(v)\beta3$ antagonists. Part III: synthesis of potent antagonists with $\alpha(v)\beta3/\alpha(IIb)\beta3$ dual activity and improved water solubility. *Bioorg. Med. Chem.* *14*, 2131–2150. <https://doi.org/10.1016/j.bmc.2005.10.055>.
 58. Kubota, D., Ishikawa, M., Ishikawa, M., Yahata, N., Murakami, S., Fujishima, K., Kitakaze, M., and Ajito, K. (2006). Tricyclic pharmacophore-based molecules as novel integrin $\alpha(v)\beta3$ antagonists. Part IV: preliminary control of $\alpha(v)\beta3$ selectivity by meta-oriented substitution. *Bioorg. Med. Chem.* *14*, 4158–4181. <https://doi.org/10.1016/j.bmc.2006.01.062>.
 59. Nunomura, S., Nanri, Y., Ogawa, M., Arima, K., Mitamura, Y., Yoshihara, T., Hasuwa, H., Conway, S.J., and Izuhara, K. (2018). Constitutive overexpression of periostin delays wound healing in mouse skin. *Wound Repair Regen.* *26*, 6–15. <https://doi.org/10.1111/wrr.12616>.
 60. Trumpp, A., Depew, M.J., Rubenstein, J.L., Bishop, J.M., and Martin, G.R. (1999). Cre-mediated gene inactivation demonstrates that FGF8 is required for cell survival and patterning of the first branchial arch. *Genes Dev.* *13*, 3136–3148. <https://doi.org/10.1101/gad.13.23.3136>.
 61. Pasparakis, M., Courtois, G., Hafner, M., Schmidt-Suppran, M., Nenci, A., Toksoy, A., Krampert, M., Goebeler, M., Gillitzer, R., Israel, A., et al. (2002). TNF-mediated inflammatory skin disease in mice with epidermis-specific deletion of IKK2. *Nature* *417*, 861–866. <https://doi.org/10.1038/nature00820>.
 62. Rios, H., Koushik, S.V., Wang, H., Wang, J., Zhou, H.M., Lindsley, A., Rogers, R., Chen, Z., Maeda, M., Kruzynska-Freitag, A., et al. (2005). Periostin null mice exhibit dwarfism, incisor enamel defects, and an early-onset periodontal disease-like phenotype. *Mol. Cell Biol.* *25*, 11131–11144. <https://doi.org/10.1128/MCB.25.24.11131-11144.2005>.
 63. Luche, H., Weber, O., Nageswara Rao, T., Blum, C., and Fehling, H.J. (2007). Faithful activation of an extra-bright red fluorescent protein in "knock-in" Cre-reporter mice ideally suited for lineage tracing studies. *Eur. J. Immunol.* *37*, 43–53. <https://doi.org/10.1002/eji.200636745>.
 64. Ge, S.X., Jung, D., and Yao, R. (2020). ShinyGO: a graphical gene-set enrichment tool for animals and plants. *Bioinformatics* *36*, 2628–2629. <https://doi.org/10.1093/bioinformatics/btz931>.

65. Seluanov, A., Vaidya, A., and Gorbunova, V. (2010). Establishing primary adult fibroblast cultures from rodents. *J Vis Exp.* 44, 2033. <https://doi.org/10.3791/2033>.
66. Uta, D., Koga, K., Furue, H., Imoto, K., and Yoshimura, M. (2021). L-bupivacaine Inhibition of nociceptive transmission in rat peripheral and dorsal horn neurons. *Anesthesiology* 134, 88–102. <https://doi.org/10.1097/ALN.0000000000003596>.
67. Kato, G., Kosugi, M., Mizuno, M., and Strassman, A.M. (2011). Separate inhibitory and excitatory components underlying receptive field organization in superficial medullary dorsal horn neurons. *J. Neurosci.* 31, 17300–17305. <https://doi.org/10.1523/JNEUROSCI.4474-11.2011>.
68. Inami, Y., Uta, D., and Andoh, T. (2020). Neuronal hyperexcitability and astrocyte activation in spinal dorsal horn of a dermatitis mouse model with cutaneous hypersensitivity. *Neurosci. Lett.* 720, 134784. <https://doi.org/10.1016/j.neulet.2020.134784>.
69. Uta, D., Oti, T., Sakamoto, T., and Sakamoto, H. (2021). In vivo electrophysiology of peptidergic neurons in deep layers of the lumbar spinal cord after optogenetic stimulation of hypothalamic paraventricular oxytocin neurons in rats. *Int. J. Mol. Sci.* 22, 3400. <https://doi.org/10.3390/ijms22073400>.

STAR★METHODS

KEY RESOURCES TABLE

REAGENT or RESOURCE	SOURCE	IDENTIFIER
Antibodies		
Rabbit polyclonal anti-periostin	In house Nunomura et al., 2018 ⁵⁹	N/A
Mouse monoclonal anti-periostin (clone SS19C)	In house Mitamura et al., 2018 ³³	N/A
Rabbit polyclonal anti-neutrophil elastase	Abcam	Cat#ab68672; RRID:AB_1658868
Mouse monoclonal anti-periostin (clone OC-20)	Sirius biotech	Cat#S-PN1
Mouse monoclonal IgM κ (clone MM-30)	BioLegend	Cat#401630
Rat monoclonal anti-F4/80 (clone BM-8)	Santa Cruz Biotechnology	Cat#52664; RRID:AB_629466
Rat monoclonal anti-Siglec-F	BD Biosciences	Cat#552125; RRID:AB_394340
Rat monoclonal anti-MCPT8	BioLegend	Cat#647402; RRID:AB_2290790
Rabbit polyclonal anti-F4/80	Abcam	Cat#ab111101; RRID:AB_10859466
Rabbit polyclonal anti-CD163	Proteintech	Cat#16646-1-AP; RRID:AB_2756528
Rabbit polyclonal anti-NF- κ B p65	GeneTex	Cat#GTX107678; RRID:AB_1951681
Goat polyclonal anti-rabbit IgG Alexa 488	Thermo Fisher Scientific	Cat#A32731; RRID:AB_2633280
Goat polyclonal anti-rabbit IgG Alexa 633	Thermo Fisher Scientific	Cat#A21071; RRID:AB_2535732
Goat polyclonal anti-mouse IgG Alexa 633	Thermo Fisher Scientific	Cat#A21050; RRID:AB_2535718
Goat polyclonal anti-rat IgG Alexa 488	Thermo Fisher Scientific	Cat#A32766; RRID:AB_2762823
Rat monoclonal anti-CD16/CD32 (clone 93)	BioLegend	Cat#101320; RRID:AB_1574975
Rat monoclonal anti-EpCAM APC (clone G8.8)	BioLegend	Cat#118213; RRID:AB_1134105
Rat monoclonal anti-CD140a APC (clone APA-5)	BioLegend	Cat#135908; RRID:AB_2043970
Rat monoclonal anti-CD31 APC (clone 390)	BioLegend	Cat#102410; RRID:AB_312905
Rat monoclonal anti-CD45.2 APC (clone 104)	BioLegend	Cat#109814; RRID:AB_389211
Peroxidase labeled polymer conjugated to goat anti-rabbit IgG	Agilent	Cat#K4003; RRID:AB_2630375
Peroxidase labeled polymer conjugated to goat anti-rat IgG	Vector Laboratories	Cat#MP-7451; RRID:AB_2631198
Biological samples		
Mouse skin	This paper	N/A
Mouse dermal fibroblasts	This paper	N/A
Chemicals, peptides, and recombinant proteins		
CP4715	Kubota et al., 2006 Ishikawa et al., 2006 ⁵⁵⁻⁵⁸ .	Provided from Meiji Seika Pharma
Mounting Medium With DAPI-Aqueous, Fluoroshield	Abcam	Cat#ab104139
Dispase I	GODO SHUSEI	Cat#386-02271
Liberase TM	Roche	Cat#5401119001
Liberase TL	Roche	Cat#5401020001
RNAiso plus	Takara Bio	Cat#9109
Recombinant mouse IL-13	BioLegend	Cat#575902
Critical commercial assays		
THUNDERBIRD® SYBR® qPCR Mix	TOYOBO	Cat#QPS201
ReverTra Ace® qPCR RT Master Mix with gDNA Remover	TOYOBO	Cat#FSQ-301
TaqMan™ Universal Master Mix II, no UNG	Thermo Fisher Scientific	Cat#4440043

(Continued on next page)

Continued

REAGENT or RESOURCE	SOURCE	IDENTIFIER
RNeasy Mini Kit	Qiagen	Cat#74104
GlycoGREEN™-βGal	Goryo Chemical	Cat#GC611
Deposited data		
Raw and analyzed data	Nunomura et al., 2019 ²⁹	GEO: GSE109936
Raw and analyzed data	This paper	GEO: GSE198169
Experimental models: Organisms/strains		
Mouse: Nestin ^{cre} ; Tg(Nes-cre)1Atp	Trumpp et al., 1998 ⁶⁰	MGI:2176835
Mouse: Ikk2 ^{ff} ; C57BL/6J-Ikbbk ^{tm2C9n} /Cnrm	Pasparakis et al., 2002 ⁶¹	RRID: IMSR_EM:01921
Mouse: Postn ^{lacZ/lacZ} ; B6.Cg-Postn ^{tm1Sjc}	Rios et al., 2005 ⁶²	RRID: MGI:5511052
Mouse: ROSA26 ^{RFP/RFP} ; B6.Cg-Gt(ROSA)26Sor ^{tm1Hlf} /leg	Luche et al., 2007 ⁶³	RRID: IMSR_EM:02112
Mouse: C57BL/6J-Nestin ^{cre} ; Ikk2 ^{ff}	Nunomura et al., 2019 ²⁹	N/A
Mouse: C57BL/6J-Nestin ^{cre} ; Ikk2 ^{ff} ; Postn ^{lacZ/+}	This paper	N/A
Mouse: C57BL/6J-Nestin ^{cre} ; Ikk2 ^{ff/+} ; Postn ^{lacZ/+}	This paper	N/A
Mouse: C57BL/6J-Nestin ^{cre} ; Ikk2 ^{ff} ; Postn ^{lacZ/lacZ}	This paper	N/A
Mouse: C57BL/6J-Nestin ^{cre} ; Ikk2 ^{ff} ; Postn ^{lacZ/+} ; Rosa26 ^{RFP/+}	This paper	N/A
Mouse: C57BL/6J-Nestin ^{cre} ; Ikk2 ^{ff/+} ; Postn ^{lacZ/+} ; Rosa26 ^{RFP/+}	This paper	N/A
Oligonucleotides		
Primers for Figures 3 and 6 see Table S4	This paper	N/A
Software and algorithms		
FlowJo (v10.7.2)	Becton Dickinson	https://www.flowjo.com/solutions/flowjo/downloads
GraphPad Prism 6.0	GraphPad Software	N/A
NDP.view2	Hamamatsu Photonics	Cat#U12388-01; https://www.hamamatsu.com/jp/ja/product/type/U12388-01/index.html
ZEN blue 3.4	Carl Zeiss	N/A
ShinyGO (v0.741)	Ge et al., 2020 ⁶⁴	http://bioinformatics.sdstate.edu/go/

RESOURCE AVAILABILITY

Lead contact

Further information and requests for resources and reagents should be directed to and will be fulfilled by the lead contact, Satoshi Nunomura (nunomura@cc.saga-u.ac.jp).

Materials availability

There are restrictions on the availability of all mouse strains, rabbit anti-periostin Ab, and CP4715 used in this study due to potential requirements for materials transfer agreements with the host institution where these materials were generated.

Data and code availability

- The CAGE dataset generated in the study has been made available in the NCBI GEO (GEO: GSE198169).
- This paper does not report original code.
- Any additional information required to reanalyze the data reported in this paper is available upon request from the [lead contact](#).

EXPERIMENTAL MODEL AND SUBJECT DETAILS

Animals

All animal experiments were performed following the Guidelines for Care and Use of Experimental Animals as required by the Japanese Association for Laboratory Animals Science (1987) and approved by the Saga University Animal Care and Use Committee (#27-051-2) and the Committee for Animal Experiments at the University of Toyama (A2020MED-6). All mice were bred in the animal facility of the Saga Medical School or the University of Toyama under specific pathogen-free conditions. Two to five mice were housed per cage under a 12-h light/dark cycle in both facilities and were given access to food and water ad libitum. Most of the experiments were performed using 4-week-old female and male mice. In some experiments for scratching bouts, motor activity, and *in vivo* extracellular recording, we used female and male mice from 4 to 16 weeks old. *Nestin^{cre}*, *Ilk2^{flf}*, *Postn^{lacZ/lacZ}*, and *Rosa26^{RFP/RFP}* mice^{60–63} were prepared by Dr. Gail R. Martin, Dr. Manolis Pasparakis, Dr. Simon J. Conway, and Dr. Hans Joerg Fehling, respectively. All mice have been backcrossed at least five generations into C57BL/6J mice and maintained on normal chow. FADS mice (*Nestin^{cre}/Ilk2^{flf}* mice) were generated by crossing female *Ilk2^{flf}* mice with male *Nestin^{cre}/Ilk2^{flf}* mice, as described previously.²⁹ FADS mice with gene manipulation of *Postn^{lacZ}* allele and/or *Rosa26^{RFP}* allele were prepared in our laboratory. Genotyping PCR of offspring from all breeding steps was performed with allele-specific primer pairs.

Preparation of primary dermal fibroblasts and dermal cells

Mouse dermal fibroblasts were isolated from skin removed from the face of the neonatal FADS/*Postn^{lacZ/+}/Rosa26^{RFP/+}* mouse (P0) as previously described.⁶⁵ Briefly, the face skin was cut, and dermal cells were dispersed with 0.14 Wunsch units/mL Liberase TM (Roche Diagnostics, Mannheim, Germany) at 37°C for 90 min. To expand the fibroblast populations, the obtained cells were cultured in DMEM/F12 media with 15% FBS for 5 to 7 days. The attached cells were collected and further cultured in a new plate with the new media for 5 to 7 days. Fibroblasts were frozen and stocked for future use when the cells reached 80 to 90% confluence. To prepare dermal cell suspensions, face skin tissues were dissected from FADS and control mice, both of which had *Postn^{lacZ/+}* and/or *Rosa26^{RFP/+}* alleles. After removing subcutaneous fat, samples were incubated at 37°C for 60 min in 1000 unit/mL Dispase I (GODO SHUSEI, Tokyo, Japan). After enzymatic treatment, the epidermal cell layer was removed from the dermal cell layer, which was then minced and further digested at 37°C for 45 min in 0.25 mg/mL of Liberase TL (Roche Diagnostics). To obtain single-cell suspensions, samples were filtered through a 40- μ m cell strainer.

METHOD DETAILS

Flow cytometry

Primary dermal fibroblasts (5×10^4) from a FADS/*Postn^{lacZ/+}/Rosa26^{RFP/+}* mouse were stimulated with or without 50 ng/mL of recombinant mouse IL-13 (BioLegend, San Diego, CA) for 24 h. To detect lacZ expression, these dermal fibroblasts and dermal cell suspensions (1×10^5) were incubated with 1 μ M GlycoGREENTM- β Gal (Goryo Chemical, Sapporo, Japan) at 37°C for 30 min. Fc blocking Ab (BioLegend) was added in experiments using dermal cell suspensions to block nonspecific binding. Then cells were labeled with the following Abs against CD45.2, EpCAM, CD31, or CD140a (BioLegend). After washing with PBS, cells were analyzed using FACSVerse and FlowJo software (Becton Dickinson, Franklin Lakes, NJ).

Immunohistochemistry and special stains

Paraffin-embedded tissue sections were prepared as described previously.²⁹ To detect eosinophils and mast cells, these sections were stained with toluidine blue or hematoxylin & eosin (HE). For immunostaining, tissue sections were incubated with 0.67 μ g/mL of anti-periostin Ab,⁵⁹ anti-neutrophil elastase Ab (1:1000; Abcam, Cambridge, UK), anti-mast cell protease 8 Ab (1:100; BioLegend), or anti-F4/80 Ab (1:100; Abcam). Peroxidase-labeled polymer conjugated to goat anti-rabbit IgG Ab (Agilent Technologies, CA) or anti-rat IgG Ab (Vector Laboratories, Newark, CA), DAB and H₂O₂ were used to detect colorimetric signals and then counterstained with hematoxylin. The distal data were obtained from stained samples using a whole slide scanner Nanozoomer (Hamamatsu Photonics, Shizuoka, Japan). The thickness of the epidermis and dermis as well as the number of eosinophils, mast cells, basophils, and neutrophils in four high-power fields ($\times 40$) were quantitatively measured with image-viewing software (NDP.view2, Hamamatsu Photonics, Shizuoka, Japan).

Immunofluorescence detection by confocal microscopy

We prepared paraffin-embedded or frozen tissue sections. Primary Abs against periostin (1 μ g/mL; clone SS19C, in-house), CD163 (1:200; Proteintech, Rosemont, IL), F4/80 (1:20; clone BM-8, Santa Cruz Biotechnology, Dallas, TX), NF- κ B p65 (1:100; GeneTex, Irvine, CA), Neutrophil elastase (1:500; Abcam), and Siglec-F (1:100; BD Biosciences, Franklin Lakes, NJ) were used for immunofluorescence analysis. Goat anti-rabbit Ab conjugated with Alexa 488 or Alexa 633, and goat anti-rat/mouse Ab conjugated with Alexa 488 were used as secondary Abs to visualize the signals. Nuclei were labeled with DAPI (Abcam). The sections were scanned using an LSM880 microscope, and the digital images were analyzed with ZEN blue image-viewing software (Carl Zeiss, Oberkochen, Germany).

Quantitative real-time PCR

Skin tissues were dissected from the face. In some experiments, we separated the skin into epidermis and dermis by treating 1000 unit/mL Dispase I (GODO SHUSEI) for 60 min. Quantitative RT-PCR was performed as previously described.²⁹ Briefly, total RNA (500 ng) was prepared from skin tissues using an RNAiso plus reagent (Takara Bio, Otsu, Japan) and reverse-transcribed with the ReverTra Ace qPCR RT Master Mix with gDNA Remover (TOYOBO, Osaka, Japan). Quantitative analyses were performed on a StepOnePlus Real-Time PCR System (Life Technologies Japan, Tokyo, Japan) using the Thunderbird SYBR qPCR Mix (TOYOBO) or TaqMan Universal PCR Master Mix (Thermo Fisher Scientific, Waltham, MA). The primer and probe sequences are shown in Table S4.

Cap Analysis of Gene Expression (CAGE)

Facial skin tissues were prepared from 4-week-old control/*Postn*^{+/+}, FADS/*Postn*^{+/+}, and FADS/*Postn*^{lacZ/lacZ} mice. Total RNA was isolated using the RNeasy Mini kit (Qiagen, Hilden, Germany). The quality of total RNA was assessed with an Agilent Bioanalyzer to ensure that the RNA integrity number was >7.0 and that the A260/280 and A260/230 ratios were >1.8. CAGE library preparation, sequencing, mapping, and gene expression analysis were performed by DNAFORM (Tokyo, Japan). Strand cDNAs were first transcribed to the 5' end of capped RNAs, attached to CAGE "bar code" tags, and then sequenced with an Illumina/Solexa Next-Generation sequencer. The sequenced CAGE tags were mapped to the mouse mm9 genomes using BWA software (v0.5.9) after discarding ribosomal or non-A/C/G/T base containing RNAs. For tag clustering, CAGE-tag 5' coordinates were input for Reclu clustering, with the maximum irreproducible discovery rate IDR at 0.1. Differentially expressed genes were selected using classical log fold-change criteria. Pathway enrichment analyses of differentially expressed genes were performed using ShinyGO (v0.741).⁶⁶

Monitoring of scratching behavior

Mice were placed individually in acrylic cages for approximately 20 min to acclimate to the conditions and were continuously kept in the same cage. Mice were recorded for at least 60 min with a video camera; scratching behaviors to the face were checked based on the recorded videos as described previously.³⁰

Drug treatment

In some experiments, FADS mice were treated with drugs such as anti-periostin Ab (OC-20) and inhibitor of integrin $\alpha_v\beta_3$ (CP4715). On day 0, we recorded scratching behaviors of 4-week-old FADS/*Postn*^{+/+} mice and then intraperitoneally injected OC-20 (200 μ g/mouse) or control IgM. After the Abs injection, video recordings of scratching behavior were made on days 1, 2, 3, 4, and 7. CP4715,⁵⁵⁻⁵⁸ provided from Meiji Seika Pharma, was dissolved in saline containing 50% DMSO and 89.5 mM HCl at 50 or 100 mg/mL and then diluted in PBS or saline. PBS or saline containing the same amount of DMSO and HCl was used as a vehicle. To assess the transient effect of CP4715, CP4715 (30 mg/kg) or vehicle was intraperitoneally administered into 4- to 8-week-old FADS/*Postn*^{+/+} mice. For long-term treatment, CP4715 (60 mg/kg) or vehicle was administered into the subcutaneous space of the back skin of 3-week-old FADS/*Postn*^{+/+} mice twice daily for 14 days.

Measurement of motor activity

Mice were trained individually in the running wheel with a counter (Cat#KN-78-M, Natsume Seisakusho, Tokyo, Japan) for 20 min per day for three days to acclimate to the experimental conditions. After the training, motor activity was measured for 60 min. To assess the sedative effect of CP4715, CP4715 (30 mg/kg) or vehicle was intraperitoneally injected into the trained mice 20 min prior to measuring.

In vivo extracellular recording from superficial dorsal horn neurons

Methods for *in vivo* extracellular recording were similar to those performed previously in the superficial spinal dorsal horn.⁶⁶⁻⁶⁸ Briefly, mice were anesthetized with urethane (1.5 g/kg, i.p.), which produces a long-lasting steady level of anesthesia that does not require additional doses. Adequacy of anesthetic depth was judged by suppression of corneal blink and hindlimb withdrawal reflexes. A laminectomy was performed exposing the cervical (C1-2) bone and the ventral portion of the occipital bone; the animal was then placed in a stereotaxic apparatus. After removing the dura and cutting the arachnoid membrane to make a window large enough to let in a tungsten microelectrode, the spinal cord surface was irrigated with 95% O₂-5% CO₂-equilibrated Krebs solution (5-10 mL/min) containing the following (in mM): 117 NaCl, 3.6 KCl, 2.5 CaCl₂, 1.2 MgCl₂, 1.2 NaH₂PO₄, 11 glucose, and 25 NaHCO₃, through glass pipettes at 37 \pm 1°C. Extracellular single-unit recordings of superficial dorsal horn neurons were performed as described previously.^{68,69} Recordings were obtained from superficial dorsal horn neurons at a depth of 10-120 μ m from the surface. Frequency (Hz) was calculated by the measurements for 30 s in all experiments. Unit signals were acquired with an amplifier (EX1; Dagan Corporation, Minneapolis, MN USA). The data were digitized with an analog-to-digital converter (Digidata 1400A, Molecular Devices, Union City, CA), stored on a personal computer with a data acquisition program (Clampex version 10.2; Molecular Devices), and analyzed with a special software package (Clampfit version 10.2; Molecular Devices).

QUANTIFICATION AND STATISTICAL ANALYSIS

The data shown are the mean \pm standard deviation (SD) or standard error of the mean (SEM). The statistical analyses were performed with Prism 6.0 software (GraphPad Software, La Jolla, CA, USA) using the two or one-sided, Mann-Whitney U-test for non-parametric data, or paired Student *t*-test for parametric data. Log rank test was used to determine the statistical significance of disease onset between *FADS/Postn*^{+/+} mice and *FADS/Postn*^{lacZ/lacZ} mice. Fisher's Exact test was used to determine statistical significance in enrichment analysis. *p* values less than 0.05 were considered to indicate statistically significant differences. Sample size (the number of animals or cells), the number of technical replicates, definitions of center and dispersion, and statistical methods for individual experiments were given in the respective figure legend.

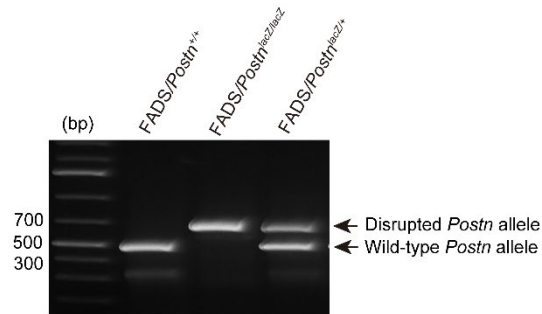
Cell Reports, Volume 42

Supplemental information

**Periostin activates distinct modules
of inflammation and itching downstream
of the type 2 inflammation pathway**

Satoshi Nunomura, Daisuke Uta, Isao Kitajima, Yasuhiro Nanri, Kosuke Matsuda, Naoko Ejiri, Midori Kitajima, Hitoshi Ikemitsu, Misaki Koga, Sayaka Yamamoto, Yuko Honda, Hironobu Takedomi, Tsugunobu Andoh, Simon J. Conway, and Kenji Izuhara

A



B

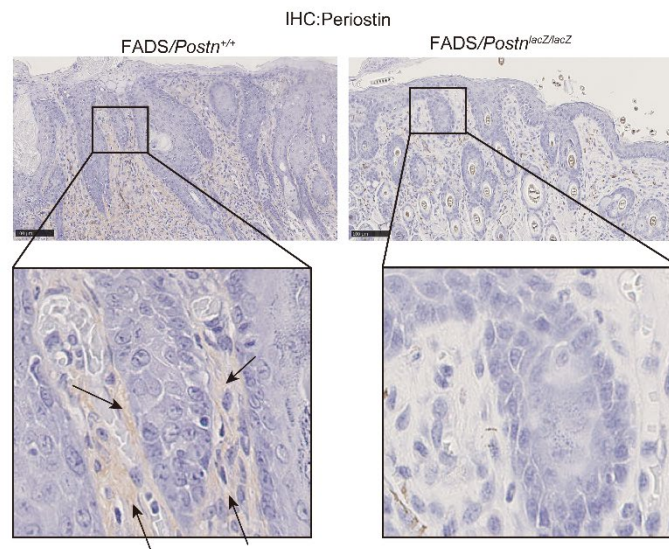


Figure S1 Disrupted periostin expression in FADS/*Postn*^{lacZ/lacZ} mice Related to Figure 3.

(A) PCR analysis of the *Postn* gene in FADS/*Postn*^{+/+} mice, FADS/*Postn*^{lacZ/lacZ} mice, and FADS/*Postn*^{lacZ/+} mice. The arrows indicate disrupted (upper) and wild-type (lower) *Postn* alleles. (B) Periostin immunostaining of the facial skin tissues of 4-week-old FADS/*Postn*^{+/+} and FADS/*Postn*^{lacZ/lacZ} mice. The expression region of periostin is visualized in brown by DAB oxidation. Arrows indicate representative expression regions in the dermis stroma of FADS/*Postn*^{+/+} mice. Scale bars: 100 μ m.

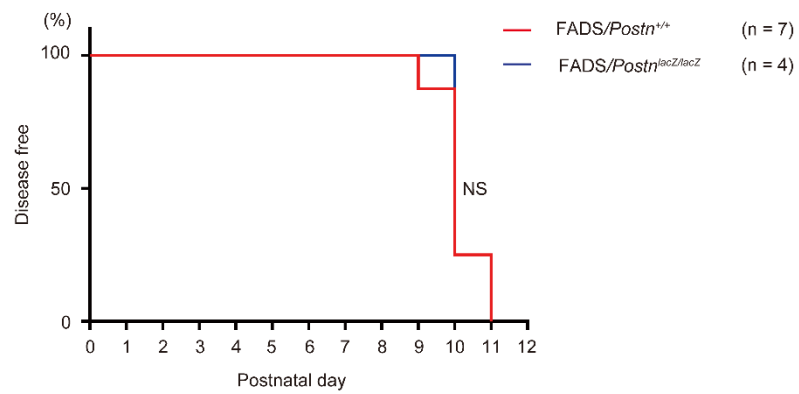


Figure S2 Periostin deficiency restricts expansion of the skin lesion area in FADS mice

Related to Figure 3.

Onset periods of facial skin inflammation in FADS/*Postn*^{+/+} mice (n = 7) and FADS/*Postn*^{lacZ/lacZ} mice (n = 4). Samples were obtained from three independent experiments. Statistical analysis was performed using a log-rank test. NS, not significant.

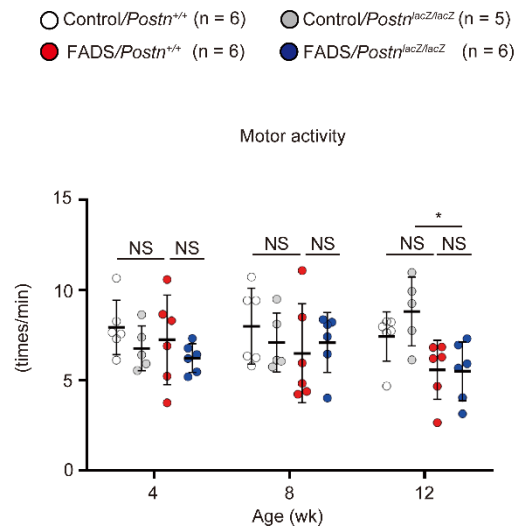
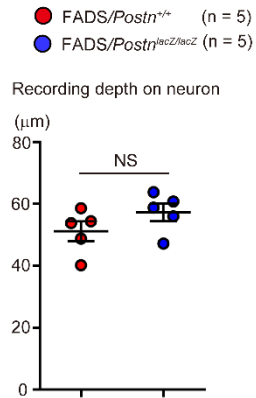


Figure S3 Periostin deficiency does not alter motor activity in FADS mice Related to Figure 5.

Motor activity on running wheels of 4-week-, 8-week-, and 12-week-old control/*Postn*^{+/+} mice (n = 6), control/*Postn*^{lacZ/lacZ} mice (n = 5), FADS/*Postn*^{+/+} mice (n = 6), and FADS/*Postn*^{lacZ/lacZ} mice (n = 6). The data shown are the mean ± SD of samples obtained from three independent experiments. Statistical analysis was performed using a one-sided Mann-Whitney *U*-test. **P* < 0.05. NS, not significant.



**Figure S4 Depth of recorded neurons in the dorsal horn
Related to Figure 5.**

Depths of recorded neurons of 8-week-old of FADS/*Postn*^{+/+} mice (n = 5) and FADS/*Postn*^{lacZ/lacZ} mice (n = 5) in dorsal horn. The data shown are the mean ± SEM of samples obtained from seven independent experiments. Statistical analysis was performed using a one-sided Mann-Whitney *U*-test. NS, not significant.

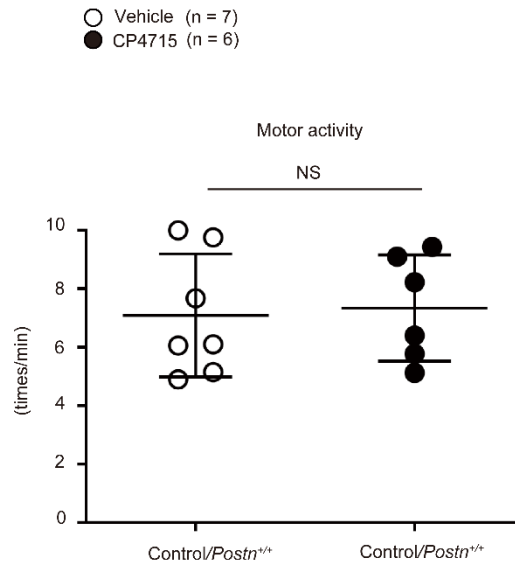


Figure S5 Effects of CP4715 on motor activity in control mice

Related to Figure 6.

Motor activities of 4-week-old control/*Postn*^{+/+} mice treated with vehicle (n = 7) or CP4715 (30 mg/kg) (n = 6). The data shown are the mean ± SEM of samples obtained from three independent experiments. Statistical analysis was performed using a one-sided Mann-Whitney *U*-test. NS, not significant.

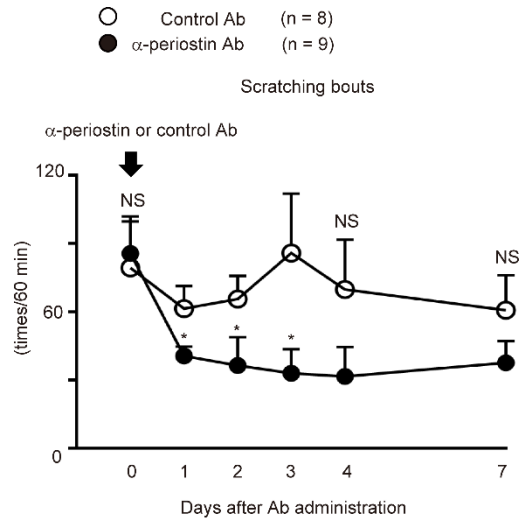


Figure S6 Effects of anti-periostin Ab on scratching bouts in FADS mice Related to Figure 6.

Scratching bouts in 4-week-old FADS/*Postn*^{+/+} mice into which a single-dose of anti-periostin Ab (OC-20, 200 μg/mouse) (n = 9) or control IgM (n = 8) was intraperitoneally administered. After the Abs injection, video recordings of scratching behavior were made on days 1, 2, 3, 4, and 7. The data shown are the mean ± SEM of samples obtained from four independent experiments. Statistical analysis was performed using a one-sided Mann-Whitney *U*-test; **P* < 0.05, ***P* < 0.01. NS, not significant.

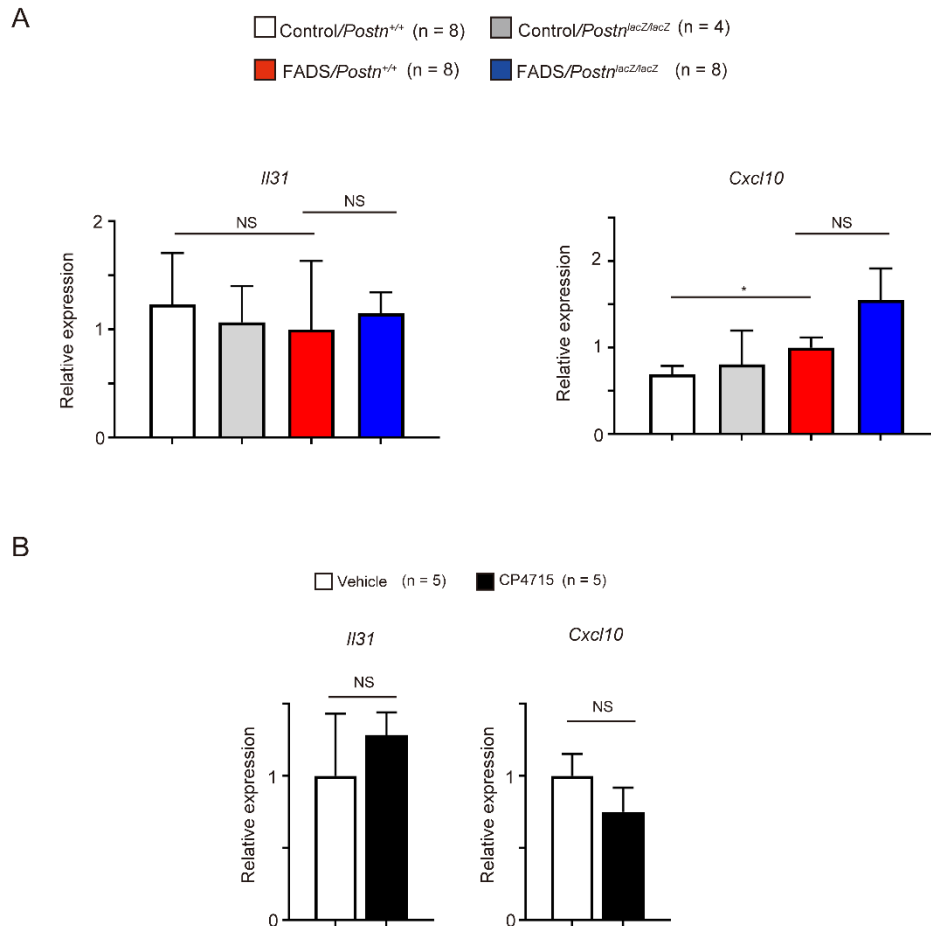


Figure S7 Effects of genetic disruption and pharmacological inhibition of periostin on the expression of IL-31 and CXCL10 in FADS mice

Related to Figures 3 and 6.

(A and B) Quantitative real-time PCR analysis for *Il31* and *Cxcl10*. (A) 4-week-old control/*Postn*^{+/+} mice (n = 8), control/*Postn*^{lacZ/lacZ} mice (n = 4), FADS/*Postn*^{+/+} mice (n = 8), and FADS/*Postn*^{lacZ/lacZ} mice (n = 8). (B) Three-week-old FADS/*Postn*^{+/+} mice were treated with continuous administration of vehicle (n = 5) or CP4715 (60 mg/kg) (n = 5) for 14 days. The relative gene expression levels were normalized to *Gapdh*. The data shown are the mean ± SEM of samples obtained from four (A) or three (B) independent experiments. Statistical analysis was performed using a one-sided Mann-Whitney *U*-test; **P* < 0.05, NS, not significant.

Table S3. Gene ontology (GO) analysis of differentially expressed genes Related to Figure 4.

Enrichment FDR	nGenes	Pathway Genes	Fold Enrichment	Pathway	URL	Genes
1.06E-24	23	62	28.89	Keratinization	http://amigo.geneontology.org/amigo/term/GO:0031424	Il1a Sprr2j-ps Krt17 Lce3b Sprr2i Sprr2d Lce3d Lce3c Sprr2h Sprr1b Sprr2b Abca12 Sprr1a Sprr2f Krt16 Sprr2k Lce3a Sprr2e Krt6a Cnfn Lce3f Lce3e Lce1k
1.27E-13	18	101	13.88	Neutrophil chemotaxis	http://amigo.geneontology.org/amigo/term/GO:0030593	Ccl3 Ccl4 Il17b Il23a Ccl20 Cxcr2 Sell Il1b Csf3r Spp1 Cxcl5 Ppbp Cxcl3 Cxcl1 Trem1 S100a8 S100a9 Cxcl2
1.87E-18	25	141	13.81	Keratinocyte differentiation	http://amigo.geneontology.org/amigo/term/GO:0030216	Epha2 Il1a Sprr2j-ps Ptgs2 Krt17 Lce3b Sprr2i Sprr2d Lce3d Lce3c Sprr2h Sprr1b Sprr2b Abca12 Sprr1a Sprr2f Krt16 Sprr2k Lce3a Sprr2e Krt6a Cnfn Lce3f Lce3e Lce1k
2.90E-13	19	123	12.03	Neutrophil migration	http://amigo.geneontology.org/amigo/term/GO:1990266	Ccl3 Ccl4 Il17b Il23a Ccl20 Cxcr2 Sell Il1b Il1a Csf3r Spp1 Cxcl5 Ppbp Cxcl3 Cxcl1 Trem1 S100a8 S100a9 Cxcl2
4.11E-12	18	124	11.31	Granulocyte chemotaxis	http://amigo.geneontology.org/amigo/term/GO:0071621	Ccl3 Ccl4 Il17b Il23a Ccl20 Cxcr2 Sell Il1b Csf3r Spp1 Cxcl5 Ppbp Cxcl3 Cxcl1 Trem1 S100a8 S100a9 Cxcl2
9.47E-12	19	150	9.87	Granulocyte migration	http://amigo.geneontology.org/amigo/term/GO:0097530	Ccl3 Ccl4 Il17b Il23a Ccl20 Cxcr2 Sell Il1b Il1a Csf3r Spp1 Cxcl5 Ppbp Cxcl3 Cxcl1 Trem1 S100a8 S100a9 Cxcl2
1.44E-15	26	209	9.69	Epidermal cell differentiation	http://amigo.geneontology.org/amigo/term/GO:0009913	Sult2b1 Epha2 Il1a Sprr2j-ps Ptgs2 Krt17 Lce3b Sprr2i Sprr2d Lce3d Lce3c Sprr2h Sprr1b Sprr2b Abca12 Sprr1a Sprr2f Krt16 Sprr2k Lce3a Sprr2e Krt6a Cnfn Lce3f Lce3e Lce1k
7.64E-11	21	216	7.57	Myeloid leukocyte migration	http://amigo.geneontology.org/amigo/term/GO:0097529	Ccl3 Ccl4 Il17b Il23a Ccr1 Ccl20 Cxcr2 Sell Il1b Il1a Csf3r Spp1 Cxcl5 Ppbp Cxcl3 Cxcl1 Serpine1 Trem1 S100a8 S100a9 Cxcl2
3.55E-13	26	276	7.34	Skin development	http://amigo.geneontology.org/amigo/term/GO:0043588	Epha2 Ctsl Il1a Sprr2j-ps Ptgs2 Krt17 Lce3b Sprr2i Sprr2d Lce3d Lce3c Sprr2h Sprr1b Sprr2b Abca12 Sprr1a Sprr2f Krt16 Sprr2k Lce3a Sprr2e Krt6a Cnfn Lce3f Lce3e Lce1k
8.09E-14	28	306	7.13	Epidermis development	http://amigo.geneontology.org/amigo/term/GO:0008544	Sult2b1 Epha2 Ctsl Cst6 Il1a Sprr2j-ps Ptgs2 Krt17 Lce3b Sprr2i Sprr2d Lce3d Lce3c Sprr2h Sprr1b Sprr2b Abca12 Sprr1a Sprr2f Krt16 Sprr2k Lce3a Sprr2e Krt6a Cnfn Lce3f Lce3e Lce1k

**Table S4. Primer sequences of genes used in qRT-PCR (SYBR green)
Related to quantitative real-time PCR in the STAR Methods section.**

Gene	Primer sequence
<i>Gapdh</i>	Forward Primer: 5' – TCACCACCATGGAGAAGGC – 3' Reverse Primer: 5' – GCTAAGCAGTTGGTGGTGCA – 3'
<i>Ccl3</i>	Forward Primer: 5' – TTCTCTGTACCATGACACTCTGC – 3' Reverse Primer: 5' – CGTGGAATCTTCCGGCTGTAG – 3'
<i>Ccl4</i>	Forward Primer: 5' – TTCCTGCTGTTTCTTTACACCT – 3' Reverse Primer: 5' – CTGTCTGCCTCTTTTGGTCAG – 3'
<i>Cxcl1</i>	Forward Primer: 5' – TGCACCCAAACCGAAGTCAT – 3' Reverse Primer: 5' – TTGTCAGAAGCCAGCGTTCAC – 3'
<i>Cxcl2</i>	Forward Primer: 5' – AGTGAAGTGCCTGTCAATGC – 3' Reverse Primer: 5' – AGGCAAATTTTTGACCGAA – 3'
<i>Cxcl10</i>	Forward Primer: 5' – TGAATCCGGAATCTAAGACCATCAA – 3' Reverse Primer: 5' – AGGACTAGCCATCCACTGGGTAAAG – 3'
<i>Ccl11</i>	Forward Primer: 5' – AGAGCTCCACAGCGCTTCT – 3' Reverse Primer: 5' – GCAGGAAGTTGGGATGGA – 3'
<i>Ccl17</i>	Forward Primer: 5' – TGCTTCTGGGGACTTTTCTG – 3' Reverse Primer: 5' – GAATGGCCCCTTTGAAGTAA – 3'
<i>Ccl24</i>	Forward Primer: 5' – GTGCCTGACCTCCAGAACAT – 3' Reverse Primer: 5' – GAGGGGATGGTCACAGAATC – 3'
<i>Il1a</i>	Forward Primer: 5' – TTGGTTAAATGACCTGCAACA – 3' Reverse Primer: 5' – GAGCGCTCACGAACAGTTG – 3'
<i>Il1b</i>	Forward Primer: 5' – CGACAAAATACCTGTGGCCT – 3' Reverse Primer: 5' – TCTTCTTTGGGTATTGCTTGG – 3'
<i>Il6</i>	Forward Primer: 5' – CATGTTCTCTGGGAAATCGTGG – 3' Reverse Primer: 5' – GACTCCAGGTAGCTATGGTAC – 3'
<i>Il17a</i>	Forward Primer: 5' – GACTACCTCAACCGTTCCACGTC – 3' Reverse Primer: 5' – TCTATCAGGGTCTTCATTGCG – 3'
<i>Il19</i>	Forward Primer: 5' – ATCCTGTCCCTGGAGAACCT – 3' Reverse Primer: 5' – CTCTCCTGATGGTCCTGGAA – 3'
<i>Il20</i>	Forward Primer: 5' – TTTTAAGGACGACTGAGTCTTTGA – 3' Reverse Primer: 5' – ACCCTGTCCAGATAGAATCTCACTA – 3'
<i>Il24</i>	Forward Primer: 5' – GCCCAGTAAGGACAATTCCA – 3' Reverse Primer: 5' – ATTTCTGCATCCAGGTCAGG – 3'
<i>Il31</i>	Forward Primer: 5' – AAACAAGAGTCTCAGGATCTTTATAACAAC – 3' Reverse Primer: 5' – ACGGCAGCTGTATTGATTCGT – 3'
<i>Il33</i>	Forward Primer: 5' – CACATTGAGCATCCAAGGAA – 3' Reverse Primer: 5' – AACAGATTGGTCATTGTATGTACTCAG – 3'
<i>Postn</i>	Forward Primer: 5' – AAGCTGCGGCAAGACAAG – 3' Reverse Primer: 5' – GGGCTGTGTCAGGAGATCTTT – 3'

**Table S4 continued. Primers and probes used in TaqMan gene expression assay
Related to quantitative real-time PCR in the STAR Methods section.**

Gene	Product number	Product number
<i>Gapdh</i>	Thermo Fisher Scientific	Mm99999915_m1
<i>I14</i>	Thermo Fisher Scientific	Mm00445259_m1
<i>I15</i>	Thermo Fisher Scientific	Mm00439646_m1
<i>I13</i>	Thermo Fisher Scientific	Mm00434204_m1
<i>Tslp</i>	Thermo Fisher Scientific	Mm01157588_m1